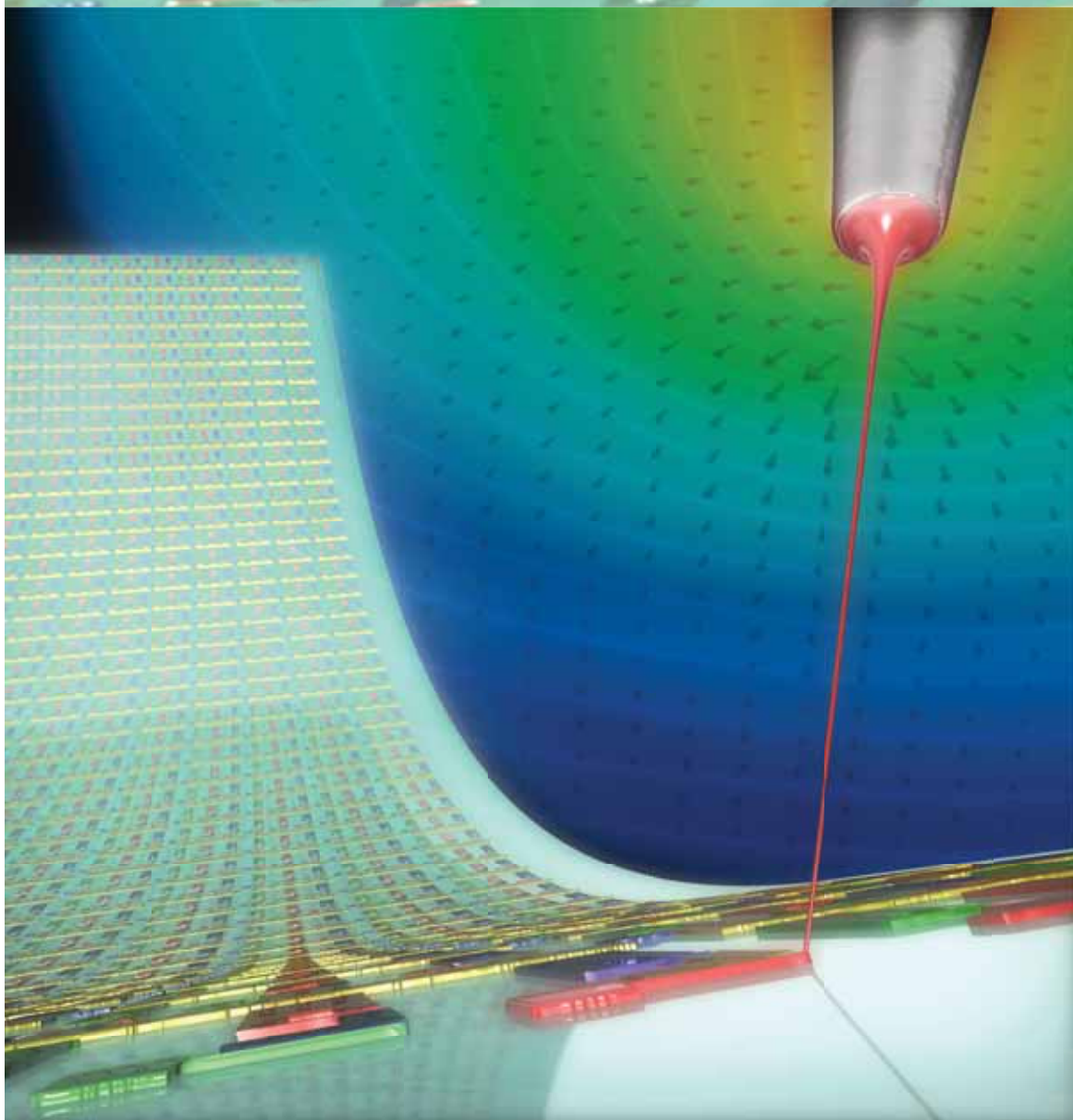


Volume 11 · No. 34 – September 9 2015

NANO MICRO

small

www.small-journal.com



34/2015

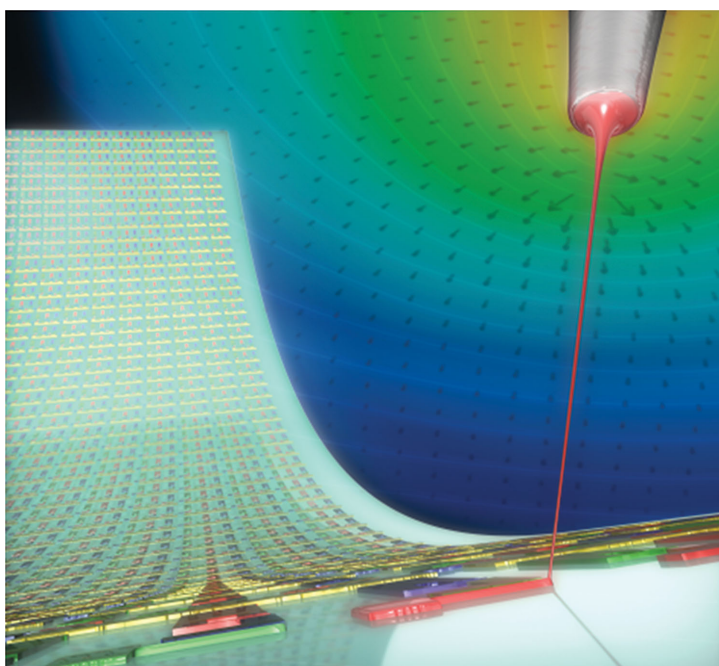
WILEY-VCH

Mechanisms, Capabilities, and Applications of High-Resolution Electrohydrodynamic Jet Printing

M. S. Onses, J. A. Rogers, and co-workers

Mechanisms, Capabilities, and Applications of High-Resolution Electrohydrodynamic Jet Printing

M. Serdar Onses,* Erick Sutanto, Placid M. Ferreira, Andrew G. Alleyne, and John A. Rogers*



From the Contents

1. Introduction	4238
2. Jet Formation and Important Factors.....	4240
3. Modifications to the Electrohydrodynamic Jet Printer	4244
4. Other Printing Techniques that Exploit Electrohydrodynamics and Related Phenomena.....	4247
5. Materials and Resolution	4249
6. Applications of E-jet Printing.....	4251
7. Concluding Remarks.....	4262

This review gives an overview of techniques used for high-resolution jet printing that rely on electrohydrodynamically induced flows. Such methods enable the direct, additive patterning of materials with a resolution that can extend below 100 nm to provide unique opportunities not only in scientific studies but also in a range of applications that includes printed electronics, tissue engineering, and photonic and plasmonic devices. Following a brief historical perspective, this review presents descriptions of the underlying processes involved in the formation of liquid cones and jets to establish critical factors in the printing process. Different printing systems that share similar principles are then described, along with key advances that have been made in the last decade. Capabilities in terms of printable materials and levels of resolution are reviewed, with a strong emphasis on areas of potential application.

1. Introduction

Techniques for fabricating structures on surfaces at micrometer and nanometer length scales are critically important to many existing and emerging technologies. The electronics industry has been the strongest driver for the development of lithographic methods as routes to dense integrated circuits that combine different materials and structures patterned at high resolution and with precise registration on semiconductor wafers.^[1] Here, size reductions translate into improved performance and increased integration density, thereby providing immense incentives to improve the fabrication processes. Today, optical lithographic techniques can fabricate features with sizes and pitches well below 100 nm. This miniaturization trend will likely continue to play a key role in sustaining advances in the semiconductor industry.^[2] At the same time, developments in other areas of application and fields of research suggest important opportunities for alternative approaches that offer complementary capabilities.^[3] Key goals here involve expanding of the diversity of materials and substrates that can be used as well as the extending of manufacturing into the third, out-of-plane, dimension. For example, the chemical and thermal sensitivities of organic and biological materials often prevent their manipulation with fabrication approaches adapted from the semiconductor industry. Additionally, flexible and stretchable substrates have emerged as important platforms for devices that integrate with the human body. In these areas as well, conventional techniques have limited utility.^[4] As a practical concern, high capital costs of advanced lithographic equipment further hinder its use in scientific research or in innovative engineering.

Additive fabrication^[5,6] approaches that rely on the localized delivery of materials of interest directly to substrates offer a solution to these challenges. This type of single-step patterning process represents a dramatic simplification compared to widely used subtractive methods, which involve repetitive deposition, patterning, and removal of materials. Additive operation also expands the selection of materials and substrates, simply because subtractive processes often introduce contamination, chemical impurities, and other forms of degradation, particularly for chemically, mechanically, or thermally fragile materials. Constraints associated with the planarity of the substrate, typically imposed by the limited depth of field in traditional lithographic techniques, are greatly relaxed in printing approaches, thereby allowing the direct formation of flexible, stretchable, or curved devices. A further inherent advantage of additive methods is in 3D fabrication: the out-of-plane dimensions of the patterned materials can be readily controlled and varied, to create options in 3D patterning of materials and in applications where thickness control is critical. The efficiency of materials utilization also has advantages, ranging from minimized waste streams to reduced costs of manufacturing.

Inkjet printing technology represents a highly established and successful additive fabrication approach, originally developed for use in graphic arts. Inkjet printing has since been adapted for applications in electronics, optics, bioengineering, and other areas.^[7–9] The process possesses all the strengths

described above for additive methods and also benefits from the tool infrastructure and knowledge developed in graphic arts applications. Inkjet printing relies on the generation of droplets at or near a nozzle aperture, followed by noncontact deposition on a substrate with high spatial control. The droplets emerge from the nozzle due to the action of pressure pulses generated, most commonly, by thermal or piezoelectric means. Simultaneous control of the ejection and location of the print head or substrate allows localized delivery of materials in layouts defined by the user. A wide variety of materials can be patterned by inkjet printing, with demonstrated applications in thin-film transistors, optical elements, organic light-emitting diodes, photonic crystals, and DNA microarrays.^[7–11] In some of these cases, inkjet printing technology is used in commercial manufacturing.

A critical challenge for inkjet printing is in the practically achievable levels of resolution. The smallest volumes of liquids that can be readily ejected from thermal/piezoelectric print heads are in the picoliter range, thereby establishing minimum sizes of patterned features as ≈ 10 micrometers.^[12] Although future research might lead to improvements, the resolution defined by the droplet size is typically further degraded by the spreading of droplets as they impact at high speeds onto the surfaces of target substrates. Besides resolution, these same issues also impose limitations on the thicknesses and spatial uniformities of the printed materials. Although these operational features are acceptable for many uses, they preclude expanded adoption for applications that require fine resolution. Some improvements are possible by modifying the wetting properties of the substrates to minimize spreading, by using inkjet printing in combination with lithographically defined chemical and/or topographical patterns, by self-aligning consecutive droplets to generate small gaps, and by engineering the inks to enhance flow from the nozzle and to minimize spreading on the substrate.^[12–14] For example, Siringhaus and co-workers demonstrated the fabrication of printed transistors with channel lengths of 5 μm and several hundreds of nanometers by using lithographically defined surface-energy patterns^[15] and a de-wetting assisted

Prof. M. S. Onses
Department of Materials Science and Engineering
Nanotechnology Research Center (ERNAM)
Erciyes University
Kayseri 38039, Turkey
E-mail: onses@erciyes.edu.tr

Dr. E. Sutanto
The Dow Chemical Company
Collegeville, PA 19426, USA

Prof. P. M. Ferreira, Prof. A. G. Alleyne
Department of Mechanical Science and Engineering
University of Illinois at Urbana-Champaign
Urbana, IL 61801, USA

Prof. J. A. Rogers
Departments of Materials Science and Engineering
Beckman Institute and Frederick Seitz Materials Research Laboratory
University of Illinois at Urbana-Champaign
Urbana, IL 61801, USA
E-mail: jrogers@illinois.edu

DOI: 10.1002/sml.201500593



self-alignment process,^[16] respectively. These methods are useful and, in some circumstances, they can generate sub-micrometer features or gaps, but they do not allow the patterning of nanoscale features in arbitrary geometries solely defined by printing and they are not generally applicable to a wide selection of materials and substrates.

Electrohydrodynamic jet (e-jet or EHD jet) printing offers a solution to the limited resolution of the conventional inkjet printer systems by exploiting different means to generate the droplets.^[17] In thermal and piezoelectric printers, it becomes impractical to eject liquids from small nozzles due to the extremely high levels of pressure required to overcome the capillary forces. While pushing fluids from a fine capillary is difficult, it is relatively easy to pull the liquids from the nozzle tip through the use of applied electric fields.^[18] As shown in **Figure 1**, e-jet printing imposes a voltage between the nozzle and an opposing conducting support to initiate the flow of inks from a nozzle via electrohydrodynamics. Typically, a back-pressure supply (e.g., syringe pump) delivers the ink to the tips of the nozzles, whose inner diameters can be as small as ≈ 100 nm. In laboratory experiments, these nozzles are typically fabricated by pulling glass pipettes and coating them with a thin layer of metal (e.g., Au), sometimes with further chemical modifications to prevent wetting of the ink on the shaft of the pipette. The electric field leads to the accumulation of mobile ions in the ink to regions near the surface of the pendant meniscus. Coulombic repulsion between these ions deforms the meniscus into a conical shape known as a Taylor cone.^[19] At sufficiently high electric fields, droplets eject from the cone as the electrostatic stresses overcome the surface tension. Although mobile charges are required, experiments demonstrate that printing is possible even with liquids that have low electrical conductivities (10^{-13} to 10^{-3} Sm^{-1}).^[20] Here the ionic mobility of the ink also plays a critical role. The simultaneous coordination of the position of the substrate and the ejection of droplets enables patterned deposition of the ink materials. Three aspects of e-jet printing allow high resolution operation: i) the inner diameters of the nozzles are smaller than those used in inkjet printing; ii) electrohydrodynamics generates droplets that can be significantly smaller than this diameter; iii) focusing due to the distribution of electric field lines minimizes lateral variations in the droplet placement.

Although only recently extended for use in micro-/nanopatterning, this concept for electric field-based printing has a long history. The electrostatic siphon recorder (1867), a tool to print telegraph messages on paper, relied on the flow of inks from a delivery tube held at a high potential relative to a grounded substrate. Similarly, Taylor described processes for the ejection of droplets under electrohydrodynamic forces almost 50 years ago.^[19] The formation of droplets from a capillary remains an active area of research due to the importance of this phenomenon in fields as diverse as electrospray deposition and the dynamics of water droplets in thunderstorms.^[21,22] Early reports^[23–25] on the use of this phenomenon for the controlled deposition of materials drew inspiration from electrospray techniques for the generation of charged droplets. In one example,^[23] electrospraying through different types of masks localized the electric field



M. Serdar Onses received his BS in Chemical Engineering and MS in Materials Science and Engineering from the Istanbul Technical University in 2006. From the University of Wisconsin-Madison, he received a PhD in Chemical Engineering in 2012. He is currently an assistant professor in the Department of Materials Science and Engineering and a co-director of the Nanotechnology Research Center at the Erciyes University. His interests include conventional and unconventional nanofabrication approaches and self-assembling materials.



Andrew G. Alleyne obtained a BS degree in Aerospace Engineering from Princeton University in 1989 and an MS and PhD in Mechanical Engineering from the University of California at Berkeley in 1992 and 1994. He currently holds the Ralph M. and Catherine V. Fisher Professorship in Engineering at the University of Illinois at Urbana-Champaign. His research includes theoretical and experimental automation and robotics related to manufacturing systems, with a focus on additive fabrication techniques for biomedical and electronic applications.



John A. Rogers obtained BA and BS degrees in chemistry and in physics from the University of Texas, Austin, in 1989. From MIT, he received MS degrees in physics and in chemistry in 1992 and a PhD in physical chemistry in 1995. From 1995 to 1997, Rogers was a Junior Fellow in the Harvard University Society of Fellows. He was with Bell Laboratories from 1997 to 2002. He is currently Swanlund Chair Professor at University of Illinois at Urbana/Champaign. His interests are unconventional materials and patterning techniques for electronics and photonics.

and hence the delivery of biological molecules to desired regions on a substrate. One of the earliest versions of e-jet printing^[24] demonstrated the formation of arrays of dots of rhodamine B with diameters smaller than $5 \mu\text{m}$. This resolution followed from the use of pulsed voltages at magnitudes smaller than those required to initiate electrospray. Aksay and co-workers performed the first systematic studies^[26,27] on the generation and placement of droplets using setups similar to the ones described above, with a demonstrated resolution of ≈ 10 micrometers, comparable to some of the best results achievable with thermal and piezoelectric inkjet techniques. Several reports^[28–31] describe electrohydrodynamic printing for graphic arts, scaffold fabrication, and conductive material patterning with minimum feature sizes greater than $10 \mu\text{m}$. Stark et al.^[32] demonstrated that an array of dots with diameters as small as $1.37 \mu\text{m}$ could be obtained using voltage-modulated printing with $4 \mu\text{m}$ inner diameter nozzles. Rogers and co-workers presented extensive demonstrations^[17,33] of

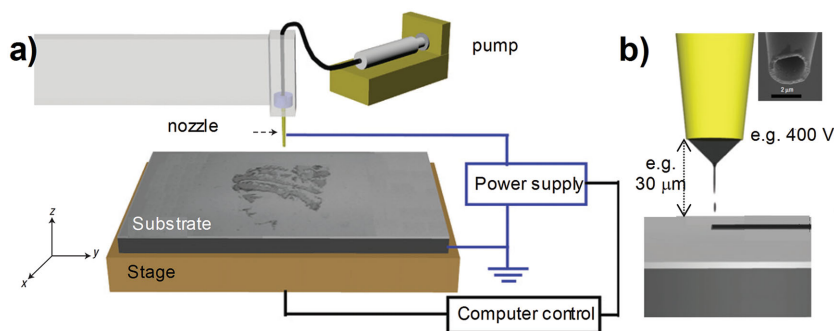


Figure 1. High-resolution, electrohydrodynamic jet printing. a) Schematic illustration of a printing system. Applying a voltage between a metal-coated nozzle (with inner diameters ranging from hundreds of nanometers to tens of micrometers) and a grounded substrate leads to the flow of inks due to electrohydrodynamic forces. A computer-controlled stage determines the location and geometry of the patterns. A syringe pump or pneumatic pressure controller provides the pressure necessary to fill the nozzle with fluid inks. b) A magnified view of the nozzle–substrate configuration. The distance between the substrate and the nozzle tip is typically in the range of tens of micrometers. Schematic illustration of the printing of a line through the movement of the stage to the right. The inset shows a scanning electron microscope image of a nozzle. Adapted with permission.^[17] Copyright 2007, Nature Publishing Group.

a range of different materials and complex pattern geometries and layouts, with resolutions extending down to 100 nm, thereby establishing e-jet printing as a high-resolution patterning approach with capabilities in nanofabrication.

This review covers recent progress in the development of advanced techniques for and applications of e-jet printing. In Section 2 the droplet generation process is described, with separate subsections on experimental and modeling studies. Section 3 summarizes various modifications to the basic e-jet printer design including multinozzle setups and desktop systems. Recently developed nanoprinting approaches that rely on similar phenomena are covered in Section 4, with individual subsections devoted to each approach. Section 5 presents a short summary of printed materials with an emphasis on advances in resolution. Section 6 provides an extensive review of e-jet printing in applications ranging from electronics to biotechnology. The final section presents a perspective on the field and its future.

2. Jet Formation and Important Factors

Understanding the physics of jet formation and determining the key parameters that affect the process are critical to high-resolution, uniform, and reproducible printing. Even though the mechanisms are conceptually simple, the actual process is quite complex and is strongly dependent on the properties of the ink such as the viscosity, surface tension, electrical conductivity, and evaporation rate.^[34] Additionally, the process is further affected by environmental- (e.g., humidity) and setup-specific factors that are often neglected. These attributes often lead to demands for careful control and optimization for each ink material. We begin by summarizing experimental studies of the dynamics of jet formation. These investigations typically use simple inks, such as pure solvents, to yield essential information on the printing process. Modeling methods that can simulate and predict the nature of jet formation for

specific sets of conditions are essential. The second part of this section highlights work in this area.

2.1. Experimental Studies on the Jet Formation Process

The electrohydrodynamic effects that cause liquids to eject from a nozzle tip, as qualitatively described in the Introduction Section, lead to different modes of jetting depending on parameters such as the strength of the electric field (E) and the flow rate (Q). The general phase diagram shown in **Figure 2a** qualitatively shows these modes and their dependence on these parameters. At low Q and E , droplets are jetted from the end of the nozzle by the help of gravitational forces in a mode called “dripping.”^[35] A slight increase in Q and/or E results in

a pulsating liquid jet where streams of distinct droplets are ejected by repeated Taylor cone formation and relaxation. “Pulsating” jets can either be achieved at Q values that are smaller than the minimum flow rate (Q_m) needed for the steady cone-jet mode or at voltages smaller than a critical value of E when $Q > Q_m$.^[36] A further increase in the electric field leads to a continuous stream of liquid from the nozzle, often referred to as the “cone-jet mode,” because of the continuous presence of the Taylor cone. The voltage at which the transition occurs from pulsating to cone-jet mode is called the Taylor, or critical, voltage, which depends on the properties of the ink and the applied back pressure.^[37] At much higher E , complex jetting behavior occurs, including tilted jets and multiple jets. Ultimately, very high E results in an atomization or spray mode. High-resolution and controllable deposition of inks favor either the pulsating jet or cone-jet mode.

These jetting modes can be observed at the end of the nozzle during printing with the use of high-speed cameras. Park et al.^[17] studied the processes of Taylor cone formation and droplet ejection in an e-jet printer using a blend of polymeric aqueous inks. They observed the pulsating jet mode at moderate ratios of E/H such as $3.5 \text{ V } \mu\text{m}^{-1}$ (H is the separation distance between the nozzle and substrate). In this mode, printing occurred via cycles (3–10 ms) of expansion and contraction of the meniscus at the end of the nozzle. In each cycle, accumulation of the ink and formation of the Taylor cone was followed by droplet ejection. This ejection relaxes the electrostatic stress on the meniscus, which subsequently contracts to its original shape. Here, the flow rate provided by the pump, the properties of the ink, and the size of the nozzle all play important roles in setting the frequency of droplet ejection. A stable jet was achieved when E/H was increased to $9 \text{ V } \mu\text{m}^{-1}$. These studies suggest that the use of sharp nozzles and low E and H values are critical in achieving high-resolution printing due to reductions in lateral deviations provided by the narrow electric-field distributions.^[17]

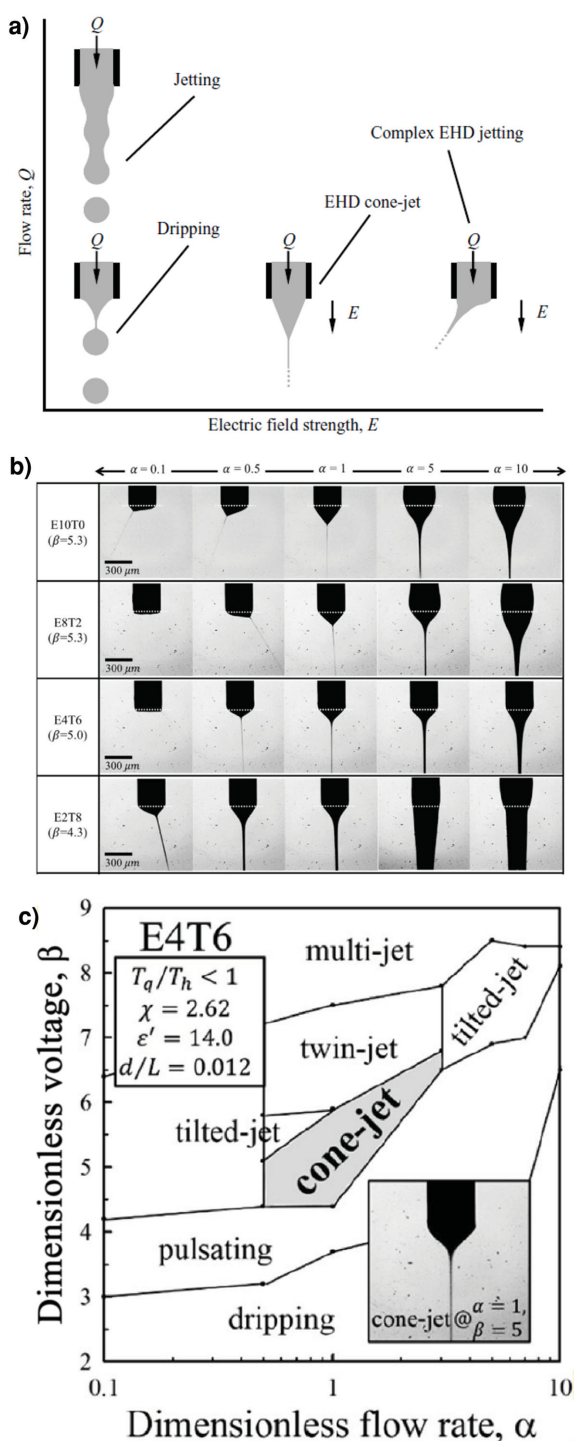


Figure 2. Formation of electrohydrodynamically induced jets under an applied electric field. a) Different modes of jetting, depending on the strength of the electric field and flow rate. Reproduced with permission.^[35] Copyright 2007, Cambridge University Press. b) Jetting behavior of mixtures of ethanol and terpineol depending on the dimensionless parameters (α : dimensionless flow rate, β : dimensionless voltage). c) Diagram showing the dependence of jetting modes on dimensionless flow parameters. Reproduced with permission.^[38] Copyright 2013, American Chemical Society.

Systematic and quantitative approaches to determining the modes of jetting for a given ink and printer setup are important for optimization. Lee et al.^[38] presented such an

approach based on dimensionless analysis and parametric maps of the jetting process. The findings identified 10 key variables related to properties of the ink, geometry of the system, and processing conditions. These variables were reduced to 6 dimensionless numbers using the Buckingham π theorem. Mixtures of pure organic solvents (ethanol and terpineol) were printed through steel capillary tubes with inner diameters of 180 μm . A high-speed camera captured images of jetting for different dimensionless numbers, as shown in Figure 2b. These images were used to construct jetting maps for different mixtures of solvents as a function of the dimensionless voltage (β) and the dimensionless flow rate (α), as shown in Figure 2c. This approach enabled a quantitative description of the different jetting modes in terms of the dimensionless numbers, thereby providing useful information for choosing the process conditions. Such jetting maps for different setups, fine nozzles, and a range of inks that contains particles, polymers, and other materials will play a key role in the continued development of e-jet printing techniques.

The pulsating jet mode has received significant interest due to its favorable properties for printing, such as the ability to deposit micro- and nanometer-sized individual droplets. Also, the conditions for this mode lie far away, in parametric space, from unwanted multi-jet and spraying modes. Here, the pulsation can either be attained using the natural frequency of the jetting or using an externally controlled, pulsed electric field. The first reports^[39] in this area focused on the frequency of pulsation that naturally occurs depending on the flow rate and electric field. Vertes and co-workers explored this frequency with an emphasis on electrospray applications and proposed scaling laws for the pulsation frequency using the capillary wave frequency spectrum of a charged droplet.^[40–42] This intrinsic pulsation was later investigated for use in high-resolution printing. Chen et al.^[27] developed scaling laws for flow rate, jet diameter, and intrinsic pulsation frequency and experimentally validated these laws using water as the ink with a 50 μm inner diameter nozzle. Choi et al.^[43] studied the effect of electric field on frequency (f) using a nozzle with an inner diameter of 30 μm and 0.1 mM KBr aqueous solution as the ink. They found that f (1–10 kHz) scales with $E/d^{1/2}$ (where d is the inner diameter of the nozzle) with ≈ 1.5 power dependence on a logarithmic scale. Another conclusion of this study was that low back pressure in the ink supply system resulted in higher frequencies and smaller droplets in comparison to the high-pressure case.

A convenient way to define the frequency of jetting and size of the droplets in e-jet printing involves the use of a pulsed electric field. The natural frequency of jetting allows limited control over e-jet printing. Here, the size of the droplets and the frequency of jetting are both coupled to the applied voltage such that they cannot be varied independently.^[44] As a solution to this limitation, researchers^[44–48] modulated the voltage with time to reach printing frequencies and droplets sizes beyond those associated with natural jetting. **Figure 3** presents an example of this approach, where pulses of high voltage are superimposed over a lower baseline constant voltage. Here, the duration of the pulse and the time between the consecutive pulses can be varied, as well as the baseline and the pulse voltages. The key to success in this

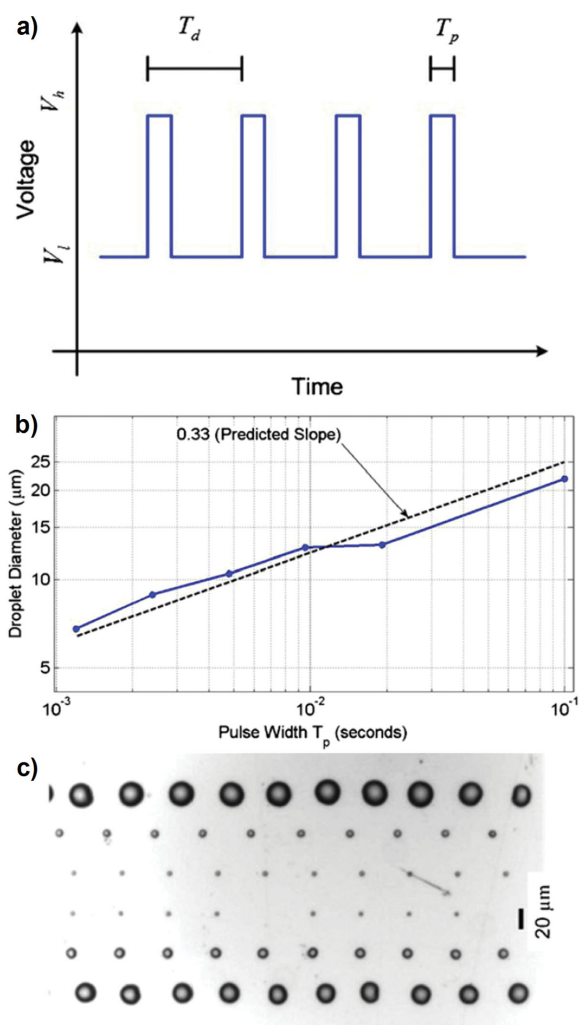


Figure 3. Drop-on-demand electrohydrodynamic jet printing. a) Illustrative temporal voltage profile for the pulsed jet. T_d denotes the time between successive pulses while T_p denotes the pulse width. V_h and V_l are the high and low voltages, respectively. b) Dependence of the diameter of the droplet on the pulse width. c) Optical microscope image showing droplets with different diameters. Reproduced with permission.^[44] Copyright 2010, IOP Publishing.

mode is the correct choice of the baseline voltage. The value should be sufficiently low such that there is no printing but sufficiently high that the cone is prepared for the pulsation. This approach enables high-speed printing of droplets, with frequencies that can reach 10–50 kHz. Stachewicz and co-workers^[47] demonstrated that the hydrodynamic phenomena inside the capillary puts an upper limit on the voltage pulse frequency. In particular, droplet ejection cannot occur effectively beyond a certain frequency that depends on the inner diameter of the nozzle. Xu et al. studied low frequency pulsation (<100 Hz) and found that the printing frequency is approximately equal to the applied pulse frequency divided by an integer that depends on the printing parameters.^[49] Additional levels of control over printing can be obtained through the use of advanced voltage pulse shapes such as sinusoids^[50] or pulses that involve more than two voltage values.^[51]

The direction of flow of the electric charges plays a key role in the jetting behavior. Most past studies used a direct current (dc) voltage such that charges flow in one direction. A significant disadvantage of dc-based e-jet systems is that a build-up of residual charges on the printed droplets can alter the dynamics of printing, particularly on insulating substrates. Byun and co-workers^[52] investigated e-jet printer systems that use alternating current (ac) modes, where the polarity switches periodically to yield zero total voltages in a time-averaged sense. Here, ejection of the droplets may happen at both the positive and negative peaks when the applied frequency of the electric field is lower than a critical value (100 Hz). In other words, the frequency of the droplet generation is two times larger than the applied frequency. It is possible to apply a combination of ac and dc voltages by superimposing one upon another. The application of a high-frequency electric field in this case may lead to the ejection of one droplet in every two cycles. Besides the frequency of jetting, the polarity of the electric field affects the behavior of the ejected droplet and may lead to deviations in droplet positioning on a substrate.^[53] In the case of a dc voltage, these deviations are typically in the form of deflections from the substrate that may lead to shifts in the positions of the droplets or satellite droplets. Such behavior is pronounced on insulating substrates, even to the extent that, in certain circumstances, the fields can cause the droplets to return to the nozzle in the case of an ac voltage. Observations of this type of effect^[52,53] used nozzles with inner diameters $\geq 200 \mu\text{m}$ and nozzle to substrate separations $\geq 1.5 \text{ mm}$. Related effects are possible with much smaller nozzles and working distances. In addition to the polarization of the electric field, different electrode structures such as plane, hole, and pin types can provide options for additional control.^[54,55] While the presence and accumulation of charges in the droplets may present challenges, the same phenomena can be used to fabricate patterns of negative and positive charges, as will be described in Section 6.6.

The electrical and chemical properties of the substrate are important to consider. Unlike conventional ink-jet methods, the electrical conductivity of the substrate is highly relevant in e-jet printing. In particular, the cumulative build-up of charge can be significant on insulating substrates, where it can distort the electric field and alter the trajectories of the droplets. These effects result in variations in the size and position of the droplets.^[53,56] While this phenomenon may provide a means^[57] to control the positions of droplets on surfaces, this phenomenon is typically unwanted in a printing process. Methods for dissipating these charges, or eliminating them entirely, range from the use of conductive substrates or substrate supports, ac fields for printing, or means to externally introduce counterions. Some applications, such as the fabrication of electrical devices, often require printing on insulating substrates, where modulation of the electric field and advanced electrode setups can be helpful, as will be discussed in detail in the next section. As for other printing processes,^[58,59] the wetting properties of the substrate play an important role in the final sizes and morphologies of the resultant features. Substrates and inks that lead to high contact angles are preferred for patterns that consist of individual

spots.^[60] Printed films and continuous lines typically require relatively low contact angles. Deng and Gomez^[61] studied the role of charge on the wetting behavior of droplets generated by electrospinning. On a conductive substrate, the droplets first spread outward to a maximum diameter and then recoil due to the surface tension. These motions are accompanied and/or followed by evaporation of solvent to lead to the final equilibrium shape and size. Charged droplets spread to a larger degree and have lower contact angles in comparison to neutral droplets. The electrical charges force the liquid to move outward in a manner that opposes surface tension.

An essential aspect of high-resolution and uniform printing relates to the properties of the nozzle. The inner diameter of the nozzle directly affects the size of droplets and is therefore a key factor in the resolution. The size of the nozzle also affects the scaling laws that govern e-jet printing.^[62] Nozzles with small inner diameters can be readily formed by pulling glass pipettes, where commercial processes allow dimensions down to 100 nm. These pulled pipettes can be coated with a thin metal layer or a metal wire can be dipped into the ink solution as an electrode for applying the electric field. An ideal nozzle surface is one that is nonwetting toward the ink materials. Since the metallic coating is inherently hydrophilic, the surface of the nozzle is often functionalized with a hydrophobic self-assembled monolayer, particularly for aqueous inks.^[17] In the absence of such a layer, a large meniscus that extends toward the outer surface of the nozzle can form.^[63] Stachewicz et al.^[64,65] found that, besides the size of the meniscus and droplets, electrohydrodynamic behavior during printing can be affected by the presence of the hydrophobic coating. Special nozzle setups such as those that involve the insertion of a nonconductive fiber inside the nozzle may be used to improve the stabilization of jets by reducing the backflow in the meniscus due to the tangential electrical stress.^[66,67]

Techniques for visualizing the jetting behavior during printing can be valuable both to research on the fundamental mechanisms and to process control. High-speed cameras and specialized optics are often used to achieve the required spatial and temporal resolution, although the finest nozzle tips and the smallest droplet sizes cannot be resolved by optical methods. A simple alternative to high-speed videography exploits strobe illumination using light emitting diodes (LEDs). Kwon et al.^[68] developed an analysis algorithm for images obtained with such a light source, to allow automatic extraction of the meniscus profile and generation of a 3D graphical representation. The data enabled the study of the effects of pulse shape on the jetting behavior. Jetting behavior can also be analyzed by tomography to reconstruct 3D profiles of the droplets using multidirectional projection data.^[69]

2.2. Modeling Studies

An enhanced fundamental understanding and computational models that can simulate the jet formation process will be needed for the practical use of e-jet printers in routine nanomanufacturing. Although the behavior of liquid droplets

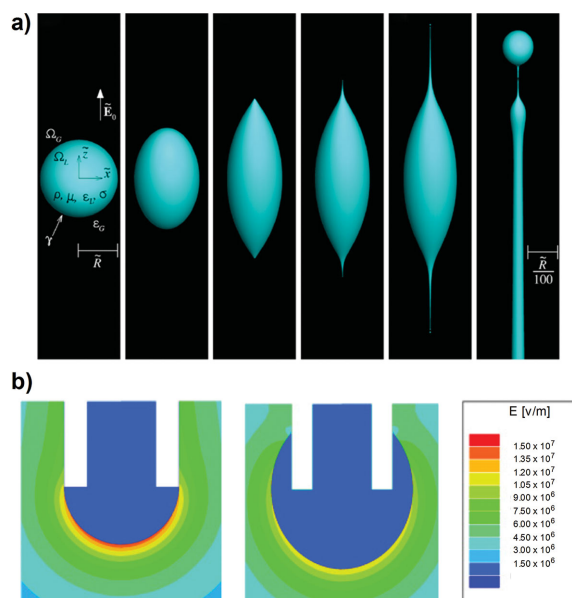


Figure 4. Theoretical studies of the process of electrohydrodynamically induced jet formation. a) Time evolution of a droplet under an applied electric field. The electric field first distorts the initially spherical drop to a spheroidal shape and then leads to formation of two Taylor cones at the ends. Later, tip streaming occurs resulting in a small droplet that disintegrates from the jet. The last image shows a magnified view of the one of the ends after tip streaming. Reproduced with permission.^[22] Copyright 2013, National Academy of Sciences. b) Distribution of electric field intensity for a hydrophobic (left) and a hydrophilic nozzle. Adapted with permission.^[63] Copyright 2010, The Japan Society of Applied Physics.

under the action of electrohydrodynamic forces has been studied since the early 20th century, several issues remain topics of theoretical study.^[70,71] Basaran and co-workers developed modeling approaches for EHD tip-streaming from a film^[72] and a droplet^[22] to capture the mechanisms of drop formation and the associated scaling laws. In a recent study,^[22] they demonstrated the existence of three different regimes for the size and charge of droplets depending on the conductivity of the fluid. The authors could simulate the time evolution of a droplet under a strong electric field, as shown in **Figure 4a**. The deformation of the drop, formation of the Taylor cone, and disintegration of the small droplets are all captured. An important aspect of such modeling studies is their ability to reveal details that are difficult or impossible to measure using experimental approaches. Higuera et al.^[73] used numerical calculations to reveal the distribution of the electrical stress on the meniscus that forms at the tip of the nozzle and different modes of pulsation as a function of time. A numerical study performed by Kim et al.^[63] explored the impact of wetting behavior of the nozzle. Calculations showed that uniform droplet ejection from hydrophobic nozzles relates to the intense fields at the tip of the meniscus (**Figure 4b**). Numerical simulation techniques developed for electrospinning can be used with slight modifications for e-jet printing. Wei et al.,^[74] for example, used a Lagrangian model to simulate electrospinning of nanoparticles on a surface and studied the effect of the spatial distribution and density of surface charges.

Post-printing processes such as evaporation of the solvent or thermal annealing may have a significant impact on the function and durability of the printed structures. In some cases, the formation of cracks results from stresses generated in the printed structures during thermal curing/cooling due to the different thermal expansion and mechanical properties of the ink and substrate. Zohdi^[75] developed a thermo-mechanical model to analyze such systems and to determine conditions that lead to compressive stresses, as a means to avoid fracture-inducing tensile stresses. Numerical simulation approaches developed for inkjet printers to measure the velocities and volume profiles of droplets can be applied to e-jet printers.^[76]

Control approaches for the automatic operation of e-jet printers must be developed in large-scale manufacturing processes. Most work has been performed in laboratory environments where the processes are manually controlled by an operator in an open-loop manner. A particular issue is in the simultaneous characterization of structures as they are printed, to provide necessary feedback for determination of parameters such as the voltage and printing speed. Two aspects of the process complicate the characterization of the printed structures. The first relates to the small length scales associated with e-jet printing: standard optical microscopy techniques become inadequate as the size of printed features extends down to 100 nm and below. A second is the short time scales associated with droplet ejection. These challenges motivate the need for control approaches that use alternative information. One option involves measurement of the current in the nozzle or substrate, immediately after the ejection or deposition of the droplet. Barton et al.^[77,78] developed control systems based on the sensing of current measured from the nozzle to maintain constant jetting frequency. Mishra and co-workers^[79] performed an extensive study on the correlation between the current measured on the substrate and the diameter and height of the printed droplets. The authors developed a model based on simultaneous high-speed camera imaging and substrate-side current measurements for three different types of inks. This model allowed the prediction of the diameters and heights of the printed droplets, with average absolute errors of $\approx 5\%$ and $\approx 10\%$, respectively. An environmental correction factor can capture the effects of the humidity and temperature of the surroundings. Iterative learning control approaches^[80,81] can further improve the repeatability in resolution and registration. Recently, Park et al. proposed two expressions to predict the size of e-jet printed dots and lines based on the contact angle of the ink.^[82]

3. Modifications to the Electrohydrodynamic Jet Printer

Printing materials from multiple nozzles allows not only the rapid patterning of structures that incorporate more than one component, but also a means for significantly increasing the total throughput of the process by parallelizing the deposition. Sutanto et al.^[83,84] designed and developed print-head systems with such capabilities, as shown in **Figure 5a**.

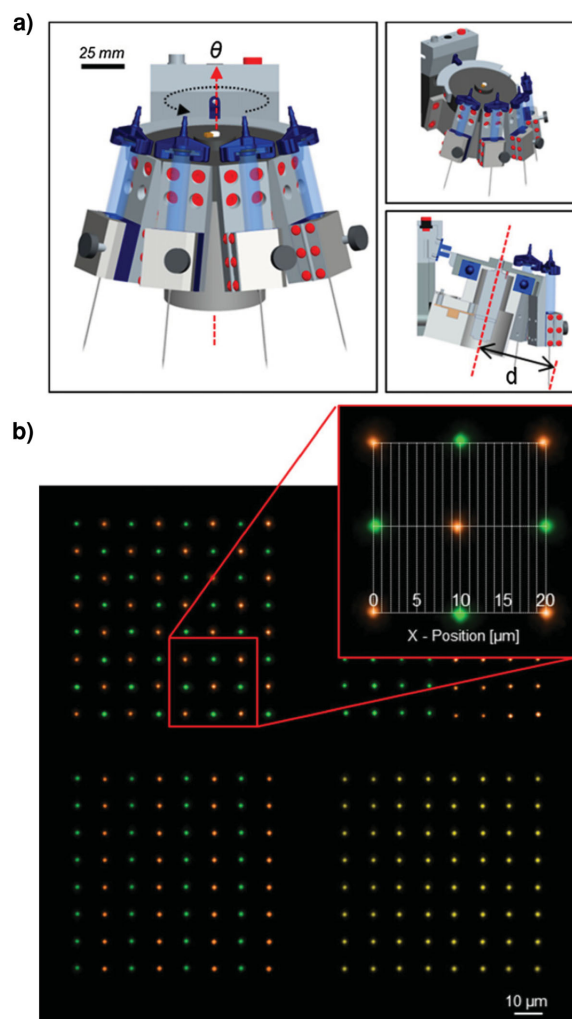


Figure 5. Multi-nozzle printing systems. a) Schematic illustration of a printing head containing multiple nozzles. b) A fluorescence image of an array of two different fluorescent molecules printed with the multi-nozzle setup. The image shows the capability to automatically align printed features within 2 μm accuracy. Reproduced with permission.^[83] Copyright 2012, IOP Publishing.

A vision-based control scheme detects the position of the nozzle with respect to the substrate, for accurate positioning of different nozzles with excellent overlay registration. Successful printing of silver interconnects and multiple fluorescent species with registration accuracy better than 2 μm can be achieved easily (Figure 5b). Such capabilities are valuable in several different application contexts, including printed electronics and biotechnology, which are reviewed in Section 6. This design can be extended to enable simultaneous printing of the same material using a tilted nozzle array.^[84] In any such scheme, electrostatic interference between the individual nozzles must be considered, as established from previous studies of electrohydrodynamic ejection of droplets from arrays of large scale nozzles.^[85–88] The small sizes of nozzles associated with high resolution e-jet printing demand a re-consideration of the electrostatics. Experiments indicated that simultaneous printing from 3 different nozzles with inner diameters of 2 μm can be performed with negligible cross-talk effects when the nozzles are separated

by more than $80\ \mu\text{m}$.^[84] On the other hand, defects such as misplaced and missing droplets appear increasingly as this spacing decreases. This limitation in the density of nozzles per unit area can be overcome by using electrode setups that deliver different electric fields to each individual nozzle. Truly high-throughput e-jet printing will require the development of approaches to fabricate print heads that contain large arrays of nozzles comparable in scale to those used in conventional ink-jet printers or developed for other direct-write systems.^[89] Initial efforts with large-scale nozzles show promise. Conventional microfabrication methods can be used to form multi-nozzle arrays for e-jet printing, as explored by several different research groups.^[90,91] In another approach, Choi and co-workers^[92,93] used a molding technique to generate a fixture made of polydimethylsiloxane for multiple glass capillaries with inner diameters of $30\ \mu\text{m}$. An interesting alternative scheme involves the use of the multi-jet mode associated with multiple openings from the same nozzle as used for electrospaying.^[94]

Improved control over the electric-field distribution between the nozzle and substrate is necessary for printing on highly insulating or rough substrates. One class of approach to manipulate the electric field uses an additional electrode with a hole between the nozzle and substrate. Lee et al.^[95] found that, with a ring-type gate electrode, the electric-field vectors can be directed toward the substrate, thereby suppressing the formation of satellite droplets that tend to occur when printing on insulating substrates. Recently, Barton and co-workers^[96] used a plate with a hole between the nozzle and substrate to direct the electric field. Plates with top and bottom conductive layers separated by a dielectric layer (Figure 6a) offered the most efficient means for shaping the electric field toward the substrate by eliminating the horizontal components. The authors found that proper choices

of the diameter of the hole, thickness and intrinsic properties of the plate, and distances between the nozzle, plate, and substrate are critical to high-resolution printing. This design allows uniform printing onto substrates that are insulating and/or have significant topography. Another route to uniform printing on insulating substrates involves modulation of the polarity of the electric field. Dong and co-workers^[97,98] studied ac-pulse modulated e-jet printing and demonstrated the patterning of continuous structures on insulating substrates such as polyethylene terephthalate (Figure 6b). Here, the frequency of the pulse, voltage magnitude, and duration can be used to control printing. Edirisinghe and co-workers^[99] investigated the effect of the print head design on e-jet printing using silk fibroin as the ink. The authors showed the ability to print lines with widths that approach $1\ \mu\text{m}$ using a design, referred to as the pinhole reservoir print head, that incorporates a nozzle with an inner diameter of $800\ \mu\text{m}$ and a second opening between the nozzle and the substrate with a diameter of $300\ \mu\text{m}$. The authors suggest that high-resolution printing from large nozzles is possible by placing the nozzle $5\ \text{mm}$ above the meniscus.

Improvements in printing capabilities can be achieved from careful design of the nozzle itself, which serves not only as a controlled opening for the flow of inks but also as one of the electrodes that generates the electric field. Nguyen et al.^[100] showed that it is possible to print using a single electrode below the substrate without a separate nozzle electrode. This configuration, which works only with ac voltage, simplifies the process by eliminating the need to establish an electrical connection to the nozzle and reduces the susceptibility to electrical breakdown. Byun and co-workers^[101] explored the use of a circular hole, referred to as a “flat” nozzle, as an alternative to the more commonly used long protruding capillary type nozzles. Although the goal was to

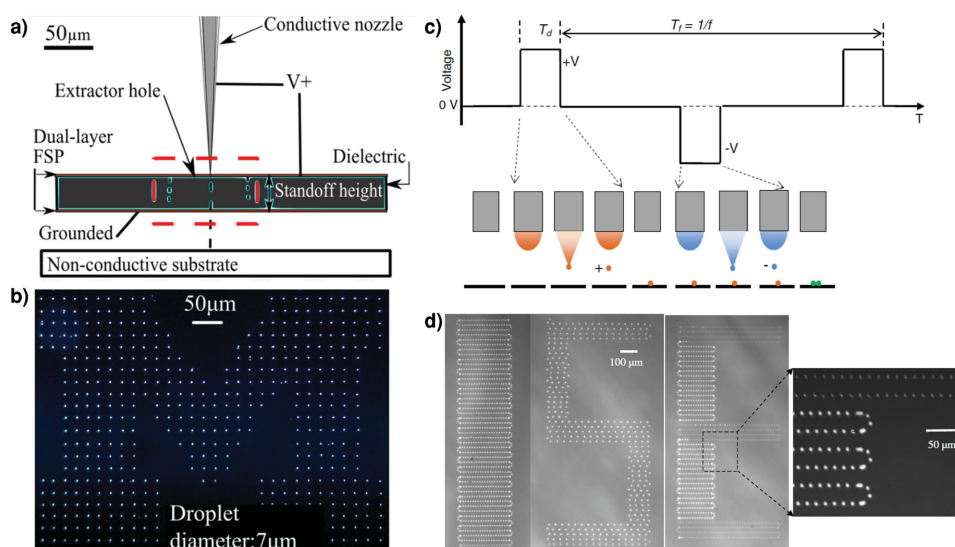


Figure 6. Printing on insulating substrates. a) Schematic description of a printing system with a double layer field shaping print head (FSP) to enable uniform patterning on insulating substrates. b) Optical microscope image showing uniform droplets with a diameter of $7\ \mu\text{m}$ printed on an insulating substrate using FSP. Reproduced with permission.^[96] Copyright 2014, American Institute of Physics Publishing. c) Schematic illustration of an ac-pulse modulated jet printing system that enables uniform printing on insulating substrates. Charge accumulation on the insulating substrate is prevented by neutralization through consecutive positively and negatively charged droplets. d) Optical microscope image of letters printed on a glass slide showing the uniformity of the generated droplets. Reproduced with permission.^[97] Copyright 2014, IOP Publishing.

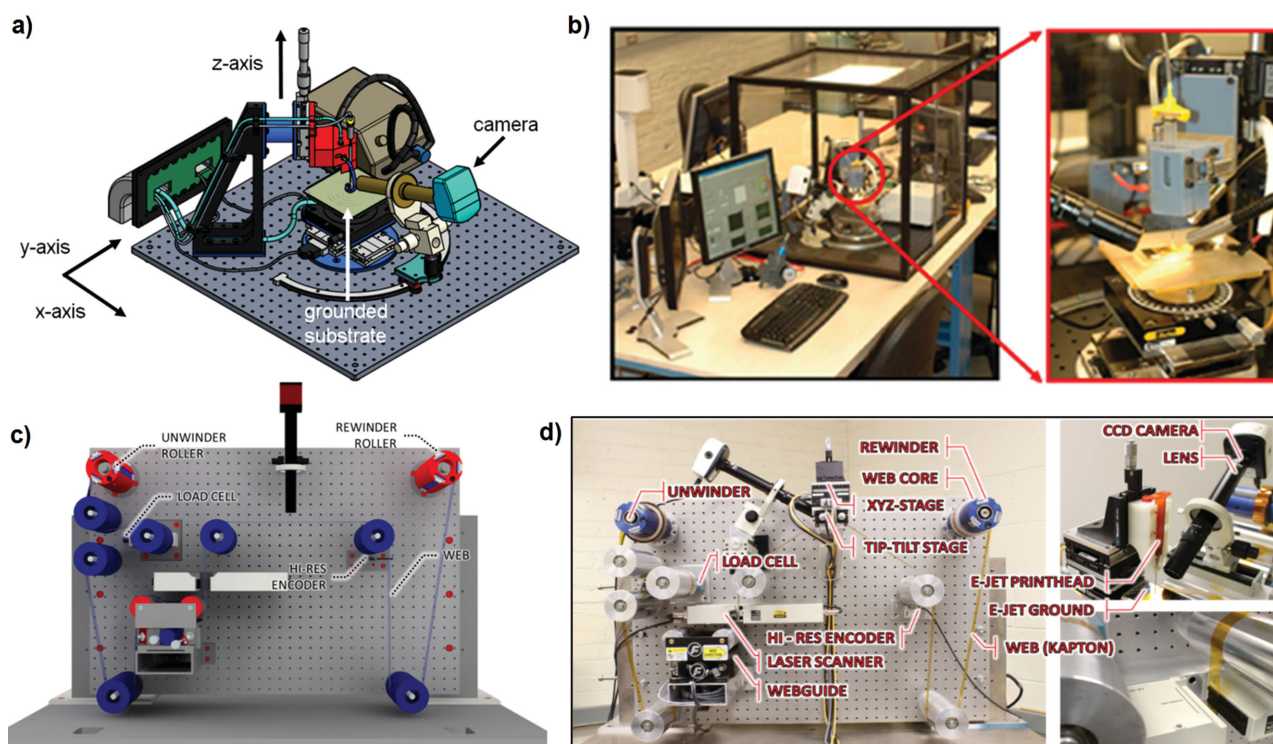


Figure 7. Design and pictures of printer systems. a) Layout and b) pictures of a small scale electrohydrodynamic jet printer system designed to fit on a typical laboratory desktop. Reproduced with permission.^[107] Copyright 2010, Elsevier. c) Schematic illustration and d) picture of a roll-to-roll electro-hydrodynamic jet printer system. Reproduced with permission.^[108] Copyright 2014 Erick Sutanto.

simplify the fabrication process, jets generated by flat nozzles are often not stable or reproducible. Improvements are possible by rendering the surface of the nozzle superhydrophobic using an argon and oxygen plasma-assisted process on a polyfluorotetraethylene film. In another effort,^[102] nozzles with inner diameters of 20 μm , and heights of 150 μm were fabricated using photolithography assisted by a glass reflow process. The high aspect ratios of the nozzles enabled the printing of structures smaller than those possible with conventional nozzles of the same size. Other studies include the use of tilted^[103] nozzles and conductive inner coatings^[104] on the capillary to access smaller length scales with an improved focusing of the electric field. The use of co-axial nozzles^[105,106] may provide additional levels of control over the structure and geometry of printed features.

The e-jet approach is amenable to printer designs that are compact, user friendly, and low cost. Most current high-resolution printers are research-oriented and involve custom-built parts, leading to issues in the reproducibility of results as well as limited access to the broader research community. Efforts at the University of Illinois at Urbana-Champaign led to the development of a desktop^[107] e-jet printer system built mostly using commercial off-the-shelf technology (**Figure 7a,b**). The hardware and user interface, including essential components such as the positioning, visualization, and electronics systems, can be purchased for a total cost of less than \$50 000. Completely assembled systems are now available commercially from other groups (e.g., <http://psolution.kr>, <http://www.sijtechnology.com>, accessed: January 2015).

Most current and previous e-jet systems operate in a batch mode on a single substrate. This approach is well matched to use with substrates such as silicon wafers or glass plates. Recent advances in flexible electronics have motivated the exploration of printing on flexible substrates. Roll-to-roll^[108–110] e-jet fabrication systems have been developed that are suitable for continuous manufacturing systems on flexible substrates (**Figure 7c,d**).

The integration of e-jet printing with other micro-/nanomanufacturing processes may provide hybrid technologies that enable new avenues of research and capabilities in applications. One possibility includes the combination of piezoelectric inkjet and e-jet printing technology.^[111–113] Here, the meniscus at the end of the nozzle is formed by a piezoelectric actuator and the droplet is ejected with the action of the electric field. Advantages of this system lie mainly in the ability to generate small droplet sizes at a high frequency using voltages that are lower than those associated with typical e-jet systems. The frequency of droplet formation is determined by the piezoelectric actuation, while the droplet size is determined by electrohydrodynamic phenomena.

Electric field-induced deposition of materials can be integrated with an atomic force microscope (AFM) cantilever for generating extremely small droplets. With a structure called the nanofountain AFM probe, Espinoza and co-workers^[114] showed that sub-micrometer features of proteins can be delivered from AFM probes by the application of an electrical potential between the probe reservoir and substrate. An integrated microfluidic system allows the continuous delivery of materials to the probes. The transport of proteins from

the probe tip to the substrate via electric field was suggested to involve electrophoretic or electro-osmotic flow. In an approach called atomic-force-controlled capillary electrophoretic nanoprinting,^[115] protein arrays that consist of bovine serum albumin were printed. The approach relied on the positioning capabilities of an AFM and electrophoretic effects to transport proteins inside a nanopipette. Both electrodes required for application of the necessary electric field were placed on the nanopipette itself, which has an opening with a diameter of 100–500 nm. Yamada and co-workers^[116,117] used an AFM cantilever modified with focused ion-beam lithography to generate an opening with a diameter of ≈ 200 nm. The deposition of the liquid was accomplished by applying a voltage bias between the ionic liquid and a conductive substrate. Droplets with diameters as small as 65 nm could be printed with this approach. In another experiment, An et al.^[118] used a pulled borosilicate nozzle with an inner diameter of 30 nm as the tip of a quartz tuning-fork AFM. They could deposit materials with widths smaller than 100 nm at a voltage bias as low as 12 V. It was suggested that the water meniscus formed between the nozzle and the surface of the substrate leads to a several-orders-of-magnitude decrease in the voltage required to print materials.

4. Other Printing Techniques that Exploit Electrohydrodynamics and Related Phenomena

The promise of using electric fields as a driver for physical mass flows in the additive patterning of materials has stimulated the development of a range of different techniques that share similar principles and/or mechanisms with e-jet printing. In this section we present a short overview of these techniques.

4.1. High-Resolution E-jet Printing Based on Autofocusing and Dielectrophoresis

Impressive feature sizes and aspect ratios in printed structures can be obtained by autofocusing droplets printed with the action of electric fields.^[119] The approach developed by Poulikakos and co-workers exploits the dripping mode, in which an applied voltage between a nozzle and a substrate leads to the periodic ejection of the droplets, as shown in **Figure 8a**. Here, gold nanoparticles with sub-10 nm diameters dispersed in n-tetradecane served as the ink. The solvent evaporates during the ejection period, thereby leading to the deposition of only nanoparticles. The novelty is that the printed structure itself functions as an electrode, to attract newly formed droplets in a manner that allows the generation of high aspect-ratio nanostructures. The authors obtained this printing regime with a working distance of 3–4 μm and nozzles with outer diameters of 0.55 μm and 1.3 μm . An interesting aspect is that printed structures as small as 80 nm are possible with nozzles that have micrometer length scales. Experimental observations and numerical calculations show

that, for voltages of ≈ 100 –300 V, increasing the voltage results in a decrease in the sizes of the features and an increase in the ejection frequency. High-resolution features can be defined at a spacing down to ≈ 100 nm, as further discussed in Section 5. In related work,^[120] the authors demonstrated that such high aspect-ratio structures can be bent due to dielectrophoretic forces associated with the application of an electric field following printing or with the interaction between the two structures.

Dielectrophoretic forces rely on inhomogeneous electric fields to enable the printing of neutral materials. Schirmer et al.^[121,125,126] investigated this mechanism for printing a colloidal suspension of gold nanoparticles (3–7 nm) in a non-polar solvent (n-tetradecane). An electric field gradient that forms near the end of the nozzle pushes the particles and the surrounding solvent, as shown in Figure 8b. The absence of Taylor cone formation during the ejection process suggests a dielectrophoretic mechanism. Arrays of dots that consist of gold nanoparticles with diameters of ≈ 175 nm are possible with this approach. Interestingly, ring-like deposits, attributed to single particles and secondary clusters present in the stream, form around these dots. Further details on the physics of the process and the effect of various parameters on the uniformity of the printed structures are reported.^[126]

4.2. Pyro-electrohydrodynamic Printing

An intriguing concept in electrohydrodynamic printing involves delivering materials to surfaces at micrometer and nanometer length scales by use of pyroelectric effects, without nozzles or electrodes. The concept, developed by Ferraro and co-workers,^[122,127,128] uses electric fields induced by local heating of a pyroelectric substrate such as lithium niobate. Here, thermal stimulation using an infrared beam or soldering iron, schematically depicted in Figure 8c, generates an electric field through the well-known pyroelectric effect. Beyond a threshold electric potential, this field pulls ink from a reservoir that rests on a second opposing substrate to form a conical jet similar to the Taylor cone. Controlling the translation of an additional substrate inserted between the lithium niobate and the opposing substrate with the liquid reservoir allows additive patterning of the ink materials. The use of drop reservoirs with small volumes allows the delivery of droplets with volumes of a few attoliters, corresponding to printed features as small as 300 nm. Numerical calculations^[129] show that electric fields similar in strength to those of conventional e-jet printers can be obtained with the pyro-electrohydrodynamic printing approach.

The use of pyroelectric effects provides new capabilities that are useful in different application contexts. In one example, the rapid curing of polymeric inks during the printing process, has allowed the fabrication of 3D structures.^[123] In particular, polydimethylsiloxane (PDMS) ink subjected to electric fields formed using the approach described above enables capture of liquid instabilities in the form of solid structures by thermal crosslinking over a duration on the order of seconds. The aspect ratio of the fabricated structures can be as high as 186, enabled by the high viscosity of the PDMS and

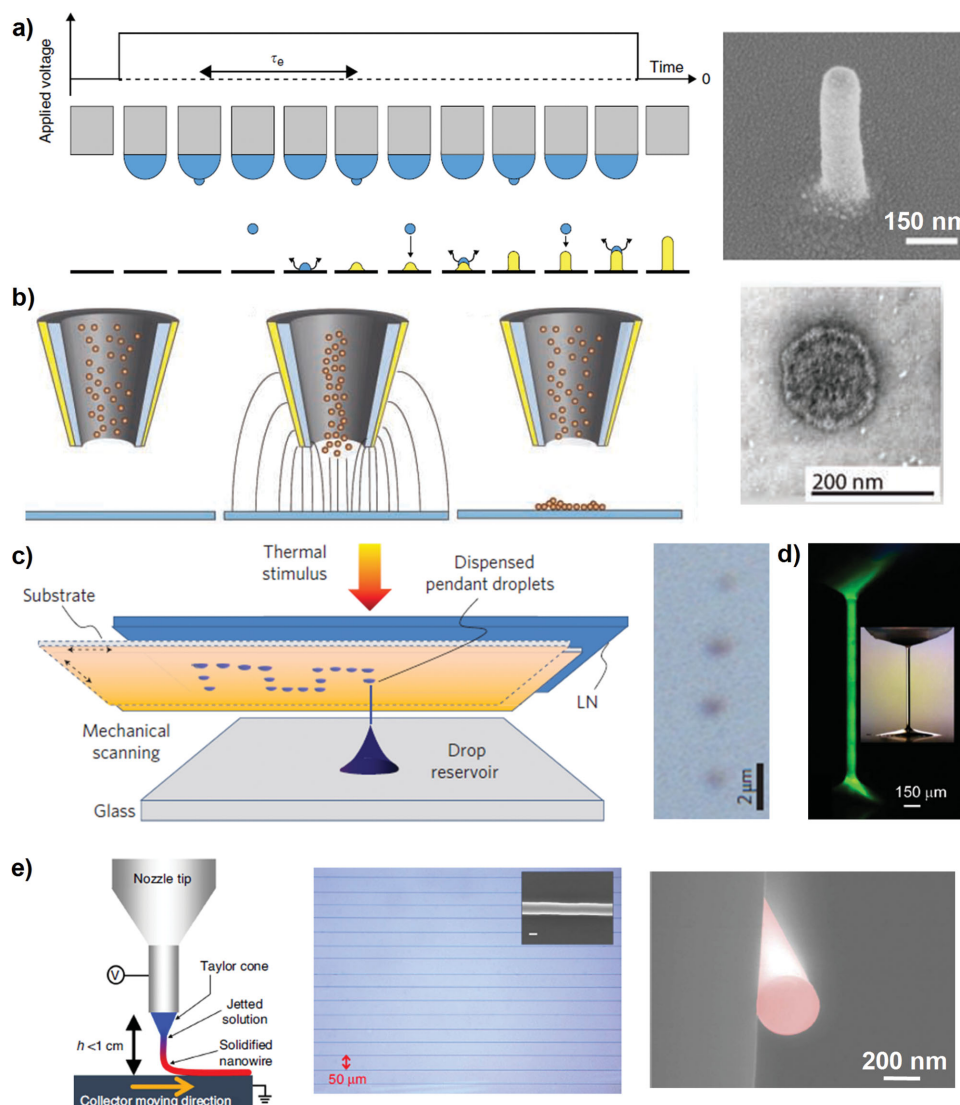


Figure 8. Other printing approaches that use electrohydrodynamic or related mechanisms. a) Schematic illustration of the electrostatic nanodroplet autofocussing (ENA) printing process. The droplets are ejected with a DC voltage at a period τ_e . The continuous repetition of this event leads to accumulation of nanoparticles. The tip of the printed structure behaves like a sharp electrode forcing the incoming droplets towards it. The inset shows a scanning electron microscope (SEM) image of a nanopillar grown with the ENA approach. Reproduced with permission.^[119] Copyright 2012, Nature Publishing Group. b) Schematic illustration of a dielectrophoretically driven process for printing uncharged polarizable particles. A DC voltage between a substrate and the tip of a fine nozzle containing a nanoparticle suspension generates a strong dielectrophoretic force on the nanoparticles. This force leads to movement and dispensing of the particles from the nozzle. The inset shows an SEM image of the printed Au dots. Reproduced with permission.^[121] c) Schematic illustration of a pyro-electrohydrodynamic printer system. A local thermal stimulus induces the pyroelectric effect in a lithium niobate (LN) substrate. This stimulus results in electrohydrodynamic effects in a thin layer of ink on the opposing glass substrate and leads to dispensing of droplets onto the target substrate. The inset shows an optical microscope image of printed droplets with sub-micrometer dimensions. Reproduced with permission.^[122] Copyright 2010, Nature Publishing Group. d) Rapid crosslinking of the polymeric structures generated by pyro-electrohydrodynamic effects enables patterning of 3D structures. Shown here is a fluorescence image of such a 3D structure. Reproduced with permission.^[123] Copyright 2011, National Academy of Sciences. e) Patterning organic nanowires based on electrohydrodynamic effects. A schematic illustration of the set-up is shown on the left. Organic nanowires are generated by operation in a near-field electrospinning mode and aligned with the controlled movement of the stage. An optical microscope and SEM image of the printed nanowires are shown, respectively. Reproduced with permission.^[124] Copyright 2013, Nature Publishing Group.

rapid cross-linking (Figure 8d). Demonstrations of the use of these structures include optical tweezers and microresonators; the latter employed quantum dots embedded in the PDMS. In another example,^[130] the fabrication of microlens arrays was shown by pyro-electrohydrodynamic printing from reservoirs of poly(methyl methacrylate) dissolved in organic solvents. A recent demonstration^[131] indicated that fibers similar to those

obtained with electrospinning can be fabricated and patterned with an adaption of this approach. Advantages of fiber fabrication in this manner include access to high-viscosity inks without clogging problems and the ability to scale up the process by using multiple ink reservoirs.

The use of electric fields to generate droplets by drawing liquids in a nozzle-free configuration can be induced in

different ways. Angelis et al.^[132] used (near infrared) NIR light sources to generate local heating in pyroelectric materials with gold nanorods as plasmonic absorbers. By comparison to far-IR sources, this development improves the ease of alignment, reduces the size, and increases the convenience and robustness of operation, all associated with the wide availability of NIR sources.

4.3. Near-Field Electrospinning

Electrospinning, a convenient process for fabricating fibers with diameters that range from several tens of nanometers up to micrometers, relies on electrohydrodynamic phenomena similar to those in e-jet printing. Highly viscous polymer solutions subjected to applied pressure forces flow through a needle, while a voltage bias between the needle and collector substrate leads to the formation of a Taylor cone and jetting. Under appropriate conditions, this jet thins and extends to a fiber due to bending instabilities. Electrospinning has been explored in a wide range of materials for different applications including reinforced composites, scaffolds for tissue engineering, textiles, and sensors.^[133] Conventional electrospinning is not suitable for applications such as the fabrication of devices where control over the position and individual alignment of the fibers is necessary. Recent work^[124,134–136] from different research groups showed that this limitation can be overcome by operating in a near-field mode and using the fast motion of the substrate. Here, decreasing the distance between the needle and collector below ≈ 1 cm reduces the whipping motion. Movement of the stage at a high speed imparts a mechanical force that leads to the alignment of the fibers (Figure 8e). Further details on this topic can be found in a recent review article.^[137] Lee and co-workers^[124,138,139] presented advanced demonstrations of this approach to fabricate electronic devices based on printed organic nanowires. Organic field-effect transistors could be fabricated with control over the position and alignment of individual fibers whose diameters were as small as ≈ 100 nm. Ahn and co-workers^[135] studied patterning of polystyrene and polydiacetylene (PDA)-embedded PS nanofibers. The diameter of the fibers varied between ≈ 60 nm and ≈ 200 nm depending on the printing conditions such as the concentration of the ink, working distance and voltage.

4.4. Other Electrohydrodynamic Processes

One of the most widely studied electrohydrodynamic processes is electrospaying, i.e., the generation of charged droplets whose size can vary from the micro- to nanoscale with a narrow size distribution. Such ionized droplets are commonly used in mass spectroscopy, particularly for the detection and analysis of large molecules such as proteins.^[140] Electrospaying shares similar physics with e-jet printing; however, the spraying effect is typically accomplished at much higher electric fields. A common usage of electrospaying is in the deposition of homogeneous thin films by directly spraying either the material of interest or a precursor which can later

decompose to form the desired product.^[141] A wide range of materials including conjugated polymers,^[142] semiconductor layers,^[143] and block-copolymers^[144] have been deposited on substrates in the form of continuous thin films with this approach. We note that the term electrospaying is also used in several different publications^[45,65,145,146] to describe general electrohydrodynamic processes (i.e., e-jet printing) which are based on the flow of materials through fine capillaries under electric fields.

Several other approaches that rely on electric fields have been developed for the additive patterning of substrates. A widely adopted method for printing hard materials such as metals and ceramics is to prepare nanoparticles of these materials and suspend them in a solvent, so that they can flow out of a nozzle. Saleh et al.^[147] developed a scheme to directly pattern materials from bulk sources using electrical discharge. Here a high voltage applied across a gap between two gold electrodes leads to electrical discharge and release of heat sufficient to melt and vaporize the electrode material. A metal tube between the electrodes and grounded substrates focuses the electric field and controls the position of deposited nanoparticles. The minimum size of features demonstrated with this approach was ≈ 50 μm . In another approach, Hong et al.^[148] used an electric field to induce a liquid bridge between the substrate and nozzle set in an inverted position. The movement of the substrate resulted in the break-up of the liquid bridge and deposition of droplets on the substrate. Electrically insulating substrates could be patterned in this approach. In a method developed by Wang et al.,^[149] local electric fields were generated with optical illumination to deliver droplets from a dielectric film in a nozzle-free configuration. Here, the optical illumination of a photosensitive layer induced local electrical stress, which led to the ejection of droplets from the film to an opposing substrate.

5. Materials and Resolution

The most recent decade of work has yielded demonstrations of e-jet printing for a diverse range of materials, with a significant emphasis on inorganic nanoparticles and organic polymers. Several criteria govern the selection of inks for electrohydrodynamically induced flows. First, the material should be in a flowable form. Solutions, suspensions, or liquid precursors that can be cured with light or temperature are good examples of candidate inks. A common approach is to dissolve/suspend the target material in a solvent to prepare a solution that can flow out of a nozzle. The use of additives can adjust the surface tension, viscosity and electrical conductivity. A second criterion is that the sizes of particles in the ink should be much smaller than the inner diameters of the nozzles. This issue is particularly important for high-resolution operation based on nozzles with openings that can be as small as 100 nm. Nozzle-free configurations and methods that use autofocusing effects as described previously relax some of these constraints in particle size. While such considerations set the prerequisites for printing, further engineering of the ink formulations is almost always necessary to find the right

combination of surface tension, viscosity, and conductivity. Details of materials can be found in the following section.

Resolution is one of the most important advantages of e-jet printing. Here we highlight some examples of the sizes of features that can be attained (Figure 9) to convey an idea of the capabilities. Early work from Park et al. showed that DNA oligonucleotides can be printed as spots with diameters as small as 100 nm using a nozzle with an inner diameter of 500 nm (Figure 9a). Subsequent studies employed special

approaches to generate features with critical dimensions below 100 nm. As mentioned previously, Poulidakos and co-workers^[119] showed that strong electric-field focusing effects enable high resolution and high aspect ratios. The authors could print fully separated linear structures down to a pitch of 100 nm and pillars with a diameter of 50 nm and an aspect ratio of 17 with this approach (Figure 9b). Work by Onses et al.^[150] demonstrated an approach to generate chemical patterns that consist of polymer brushes with feature sizes well below 100 nm. This study implemented e-jet printing in a near-field electrospinning mode to form fibrous polymer structures rather than isolated droplets. The patterned polymer brushes had feature sizes much smaller than the inner diameter of the nozzle. For example, line-widths as small as 50 nm were possible as shown in Figure 9c using a nozzle with an inner diameter of 1 μm . The resulting pattern was sufficiently small to influence the self-assembly of block copolymer domains with widths of ≈ 40 nm. Finally, Figure 9d presents an example of an array of spots with diameters that are less than 50 nm via electric field assisted printing from a hollow AFM tip.^[117]

Different strategies can be employed to pattern features with diverse geometries using e-jet printing. Dots constitute the most basic structure, and can consist of either isolated droplets or multiple coalesced droplets. The location of the droplets can be controlled with the movement of the stage in synchronization with the applied voltage, either in a mode of continuous pulses or in individually actuated droplets followed by each movement. The latter provides exact control over the positions of droplets, but can be relatively slow. Line patterns can form as a result of the coalescence of the individual droplets through a suitable combination of proper stage speeds and wetting of the substrate by the ink. Finally, continuous films can be obtained by raster scanning lines in a defined area. Here, over-lapping lines result in continuous films below certain spacings between adjacent lines. The thickness of the printed film typically scales linearly with the

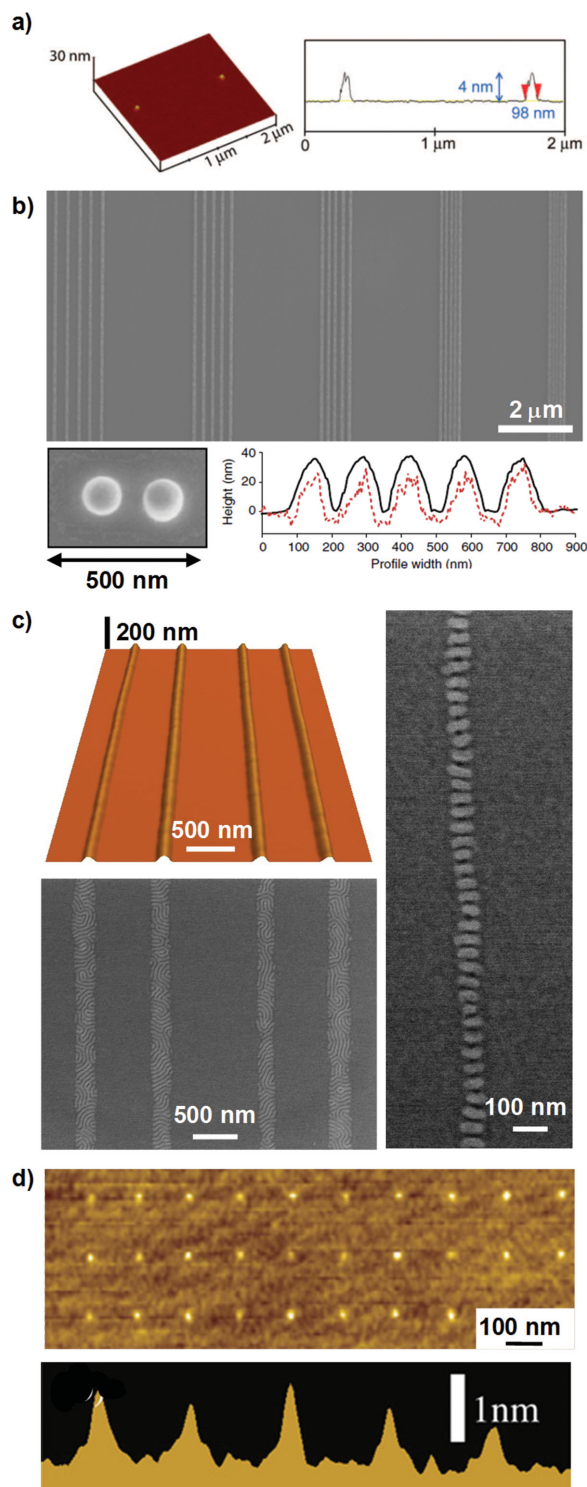


Figure 9. Nanoscale resolution in printing. a) DNA oligonucleotide dots with average diameters of ≈ 100 nm. An AFM image (left) and a height profile of the printed dots. Reproduced with permission.^[33] Copyright 2008, American Chemical Society. b) Printed gold nanostructures with varying pitch (250, 200, 150, 100 and 75 nm) are shown in the top SEM image. The height profiles of the printed nanostructures are shown at the bottom right. A magnified view of gold nanopillars printed with the autofocusing approach is given at the bottom left. Reproduced with permission.^[119] Copyright 2012, Nature Publishing Group. c) High-resolution chemical patterns consisting of polymer brushes with feature sizes below 100 nm. The top left is an AFM image of printed polymer brushes before grafting and washing. The resulting chemical patterns lead to perpendicular assembly of block-copolymer films as shown in the SEM image (bottom left). Line widths as small as ≈ 50 nm are possible, as shown in the SEM image (right). This line width results in the alignment of the polymer domains. Reproduced with permission.^[150] Copyright 2014, American Chemical Society. d) Electric field-assisted deposition of inks from a hollow tip using dynamic mode AFM. Shown are an AFM image (top) and a height profile (bottom) of the printed structures. The diameters of the printed spots are less than 50 nm. Reproduced with permission.^[117] Copyright 2012, American Institute of Physics Publishing.

inverse of this spacing. Previous research showed that highly uniform printed films with a roughness smaller than 2 nm is possible using e-jet printing.^[151]

6. Applications of E-jet Printing

6.1. Printed Electronics

One of the most prominent areas of application for e-jet printing is in the fabrication of electronic devices. Printed electronics is an emerging field that is expected to reach a market value of several hundred billion dollars.^[152–155] Several different considerations motivate the development of this industry: i) There is strong interest in unusual forms of electronics devices that can be worn or integrated with the human body; these require fabrication approaches that are compatible with flexible/stretchable substrates and curved or structured surfaces; ii) some active materials (i.e., organic semiconductors, biomaterials for sensing) are chemically, mechanically, or thermally incompatible with traditional approaches from the existing semiconductor industry, such as photolithography; iii) there is a need for low-cost and environmentally friendly fabrication of electronic devices where the material usage is minimal. Ink-jet printing technology represents a leading fabrication approach for this area, and is already used by several companies. As with conventional electronics, reductions in critical device feature sizes decrease operating voltages, increase switching speeds and increase levels of integration. E-jet printing has a strong potential to extend these trends by enabling structures in printed electronics at sub-micrometer and nanometer length scales.

6.1.1. Printing Conductive Materials

One challenge in printed electronics is to define device components such as interconnects, electrodes, and contact pads with sufficient resolution and electrical conductivity. Conducting inks must offer properties (e.g., viscosity, surface tension) that allow flow through the tips of fine nozzles. These requirements focus research on inks that exploit metal nanoparticles, carbon nanotubes, and other conductive nanomaterials. Extensive reviews on such inks for printed-electronics applications can be found elsewhere.^[153,156,157] Silver nanoparticles are the most widely studied material for patterning conductive tracks by e-jet printing.^[158–168] A common approach is to use silver nanoparticles suspended in an organic solvent as the ink. A subsequent thermal process sinters the particles into continuous metal structures. This heating step removes ligands that cover the nanoparticles, to allow their coalescence into a dense structure. The process involves interactions between the ligands and the metal surfaces as well as the adsorption and transfer of heat through and between the particles.^[169,170] To achieve necessary thicknesses, it is often necessary to print repetitively in the same targeted area. As in the case of other materials, the properties of the ink as well and the relevant printing conditions are important in achieving uniform structures. Byun and co-workers performed a detailed study of the uniformity of e-jet

printed silver dots and explored the effects of surface energy and temperature of the substrate.^[166] Using a commercially available silver nanoparticle ink in butyl-carbitol and a nozzle with an inner diameter of 6 μm , the authors generated silver dots with diameters between 7 μm and 20 μm . As shown in **Figure 10a**, the process allows for generation of uniform arrays of Ag dots with diameters less than 10 μm . The use of low surface energy (hydrophobic) and high-temperature substrates coupled with repeated printing on the same spot increases the height of structures and suppresses any coffee-ring effects and other sources of nonuniformities. Rahman et al.^[167] showed that overlapping such droplets can define continuous linear structures that are suitable as interconnects in electronic devices. The diameters of the droplets could be varied from 3.8 μm to $\approx 100 \mu\text{m}$ using a nozzle with an inner diameter of 10 μm , by controlling printing conditions such as the pulse time, applied pressure, and voltage. The authors found that uniform lines result when the spacings between the individual droplets are less than $\approx 70\%$ of their diameters. The widths of the lines depends linearly on the diameters of the droplets (**Figure 10b**). Arrays of uniform lines with widths of 6.5 μm were successfully printed on insulating glass substrates. In a recent study by Son et al.,^[168] the effects of repeated printing and sintering of printed silver lines were explored, as well as the influence of printing parameters such as the working distance, stage speed, and applied voltage range. Here, repeated printing over the same line resulted in an increase in the thickness of the line without significant change in the width. Nevertheless, the uniformity of the thickness across the width of the line decreased (**Figure 10c**). With the use of laser sintering, the authors patterned metal lines with widths of 3 μm and heights of 230 nm, and an electrical resistivity less than 20 $\mu\Omega\text{cm}$. Hybrid electrodes can be fabricated by printing silver nanoparticles on graphene for achieving low sheet resistance and high optical transmittance necessary for transparent heaters.^[171] Reports on the fabrication of silver electrodes on curved glass^[172] and flexible polyethylene terephthalate^[173] substrates show the promise of e-jet printing for fabrication of unusual electronic devices.

Recent efforts have focused on copper and aluminium nanoparticles, as a low-cost alternative to silver. Choi and co-workers^[174,175] explored e-jet printing of copper nanoparticles with average diameters of 40 nm. Nozzles with inner diameters of 60 μm yielded copper lines with widths of 12 μm and resistivities of $2.42 \times 10^{-7} \Omega\text{m}$ (**Figure 10d**). Synthetic routes exist^[176] to prevent the formation of copper oxide through the use of passivation layers. In another effort, Yoon and co-workers^[177,178] explored e-jet printing of aluminum particles with diameters in the micrometer length scale. The authors demonstrated the printability of these inks but with a relatively coarse resolution due to the large particle sizes. Alternatively, microstructures may be fabricated through the combined use of e-jet printing with conventional etching processes.^[179]

6.1.2. Transistors

As the most fundamental element of electronic circuits, the fabrication of transistors using e-jet printing has received significant attention. In one effort, Paik and co-workers^[180]

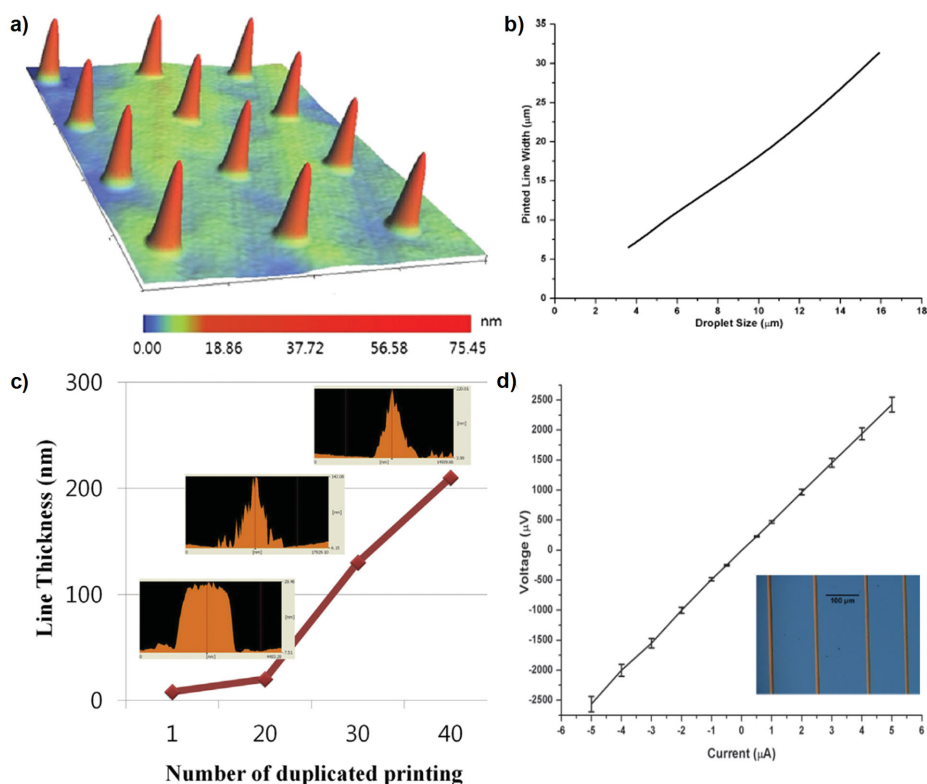


Figure 10. Silver nanoparticles for printed electronics. a) An array of Ag dots generated by electrohydrodynamic jet printing a suspension of Ag nanoparticles. Shown is an AFM image of dots with a pitch of $\approx 40 \mu\text{m}$. Reproduced with permission.^[166] Copyright 2013, IOP Publishing. b) The width of the line as a function of the diameter of the droplets. Droplets consisting of Ag nanoparticles can form lines necessary for electrical interconnects. Reproduced with permission.^[167] Copyright 2013, Springer. c) The plot shows the relation between the thickness of the printed Ag lines and the number of passes over the same. Reproduced with permission.^[168] Copyright 2014, Elsevier. d) Current-Voltage (I - V) curve of printed conductive tracks. The width of the line is $12 \mu\text{m}$. The lines were generated by printing a suspension of Cu nanoparticles. Reproduced with permission.^[174] Copyright 2012, IOP Publishing.

fabricated thin-film transistors by patterning amorphous oxide semiconductors using e-jet printing. Indium zinc oxide served as the semiconductor and was printed from a precursor solution that contained indium nitrate hydrate, zinc acetate dehydrate, 2-methoxyethanol and mono-ethanolamine. The authors demonstrated line widths as small as $1.5 \mu\text{m}$ using a nozzle with an inner diameter of $2 \mu\text{m}$, enabling transistor fabrication at a $10 \mu\text{m}$ length scale. **Figure 11a** presents a schematic depiction and characterization results from thin-film transistors fabricated with this approach. While serpentine patterns were patterned using e-jet printing, source and drain electrodes were defined by photolithography and a lift-off process. The devices displayed mobilities of $3.7 \text{ cm}^2\text{V}^{-1}\text{s}^{-1}$ and on/off current ratios better than 10^5 . In another example,^[181] e-jet printed patterns of indium gallium zinc oxide precursor solutions with formamide as a cosolvent were used in thin-film transistors. The incorporation of formamide resulted in an increase in the field-effect mobility. In another demonstration, Jeong et al.^[176] fabricated graphene-based thin-film transistors using e-jet printing. Here, source and drain electrodes were defined by printed copper nanoparticles; graphene served as the channel as shown in **Figure 11b**. The transistors showed ambipolar behavior with hole mobilities of $1260 \text{ cm}^2\text{V}^{-1}\text{s}^{-1}$. The fabrication of zinc-tin oxide transistors with channel widths of $60 \mu\text{m}$ have also been

reported.^[182,183] Organic transistors with channel lengths of several micrometers can be achieved by directly printing metallic nanoparticle on top of the organic layers.^[184]

6.1.3. Memristors

Another electronic circuit element of interest is the memristor, a two-terminal device in which the resistance can be reversibly switched with appropriate voltages. Choi and co-workers^[185,186] demonstrated a flexible memristor device fabricated by e-jet printing. The cross-bar structure shown in **Figure 11c** consists of an active layer of zirconium dioxide sandwiched between bottom and top silver electrodes. This structure was printed on a flexible polyimide substrate using a dispersion of silver and zirconium dioxide particles as the ink in a cone-jet and spraying mode, respectively. The devices retain sufficient on/off ratios after 100 cycles of switching and 500 cycles of mechanical bending. Memristors can also be printed with copper and titanium dioxide as the bottom electrode and active layer, respectively.^[187]

6.1.4. Display Devices

E-jet printing may also find use in the fabrication of displays. In one effort, Byun et al.^[188] showed that e-jet

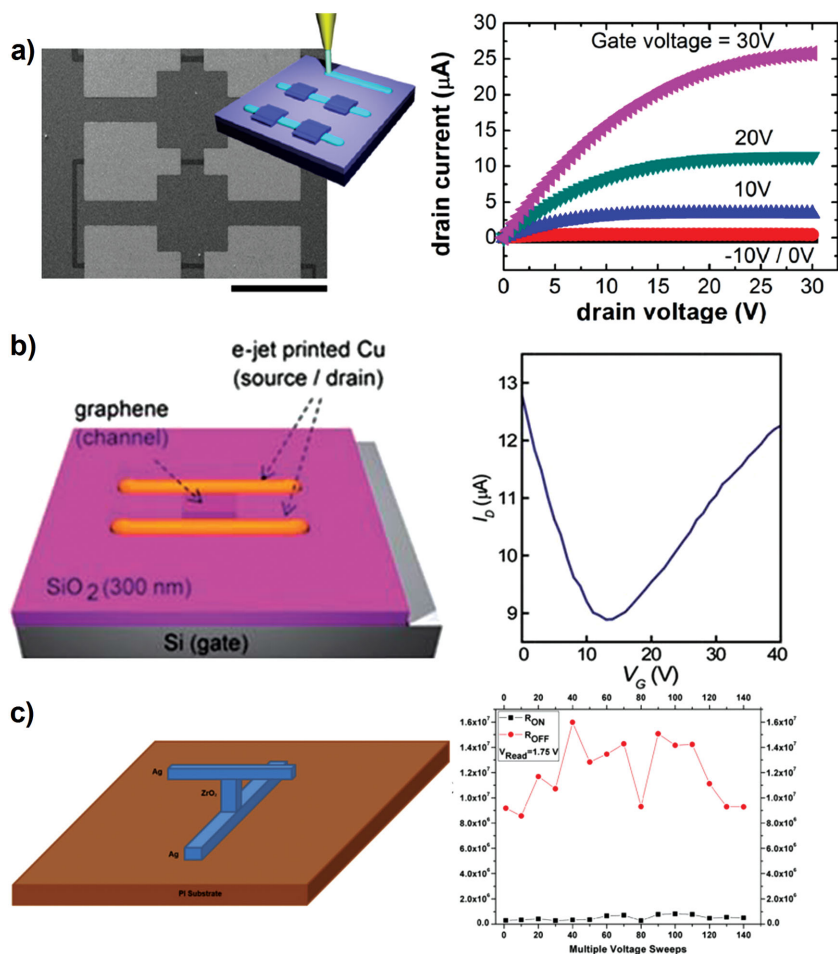


Figure 11. Fabrication of electronic devices with electrohydrodynamic jet printing. a) Schematic illustration of the fabrication of thin film transistors (TFTs) with printed indium zinc oxide (IZO) semiconductors and an SEM image of the device. Scale bar: 400 μm . The IZO channels were defined by printing and the source and drain electrodes were patterned by photolithography. Representative output characteristics of the device are shown on the right. Reproduced with permission.^[180] Copyright 2012, American Institute of Physics Publishing. b) Schematic illustration of graphene TFTs with printed Cu electrodes. The graphene layer serves as the channel and the printed Cu as the source/drain electrodes. The plot on the right shows source/drain current (I_D) versus back-gate bias (V_G). Reproduced with permission.^[176] Copyright 2013, The Royal Society of Chemistry. c) Schematic illustration of the fabrication of a memristor by electrohydrodynamic jet printing. ZrO_2 layer and the Ag electrodes were defined by printing. Effect of multiple voltage sweeps on the resistance of the fabricated device is given on the right. Reproduced with permission.^[185] Copyright 2013, Elsevier.

printing technology can define alignment layers in liquid crystal displays as a replacement for the conventional spin-coating process. Here, polyimide was printed in a multi-jet mode at a thickness of 50 nm, followed by thermal annealing and mechanical rubbing. The results indicate that the alignment properties of liquid crystals on such films are as good as those on films cast in the usual way. The potential of e-jet printing for the patterned deposition of polyimide may provide additional capabilities. Park et al.^[189] explored the use of e-jet printing to pattern spacers to define the gap distance between the transistor and color filter substrates. The authors fabricated the spacer by printing a negative tone photolithography resist (SU-8). The transmittance and thermal stability of the printed spacer showed promise as

a substitute for the current materials and processes. Other elements of displays such as color filters can also be fabricated with e-jet printing. In an effort towards this goal, Ahn and co-workers investigated carbon black as an ink for e-jet printing.^[190] Another possible use of e-jet printing could be in repair of the defects that are present in flat panel displays.^[191]

6.2. Sensors

E-jet printing may find additional application in sensing platforms. E-jet printing can not only be used to fabricate whole sensors, but also for site-specific delivery of analytes to enable capabilities that are not present in conventional systems. **Figure 12** presents several such demonstrations. Song et al.^[192] prepared arrays of dots and lines that consist of porphyrin, of interest for sensing applications due to its high selectivity and quick response to different gases. The authors showed that the fluorescence from patterned porphyrin arrays decreases to low levels in the presence of nitric acid vapor, there by presenting a route to acid sensing. Choi et al.^[110] fabricated a temperature sensor on a flexible poly(ethyleneterephthalate) substrate by e-jet printing silver nanoparticles. The sensor shown in Figure 12a consists of a series of connected silver lines and operates based on the measurement of resistivity changes that depend linearly on the temperature. Pikul et al.^[193] e-jet printed polymer droplets on a microcantilever sensor, which offers high sensitivity detection of various analytes through changes in the mechanical resonance of the cantilever (Figure 12b). An advantage of this approach is in the ability to deposit multiple analytes at a high resolution. An important additional

aspect of this study was the use of a heated nozzle to melt polymer inks that exist as solids at room temperature. A similar approach was used to determine the viscoelastic properties of microstructured hydrogels, of interest for biomedical applications. As depicted in the 3D reconstructed image of Figure 12c,^[194] e-jet printing provided high-resolution placement of polymer droplets on resonant sensors based on a microelectromechanical system (MEMS). E-jet printing has additional promise in the fabrication of high-temperature MEMS sensors made of ceramics, where polymer solutions serve as inks that are precursors to ceramics.^[146] In another example, biomolecules printed onto the surface of a silicon photonic crystal provides enhanced fluorescence and sensitive detection from biomarkers (Figure 12d).^[195] An area of

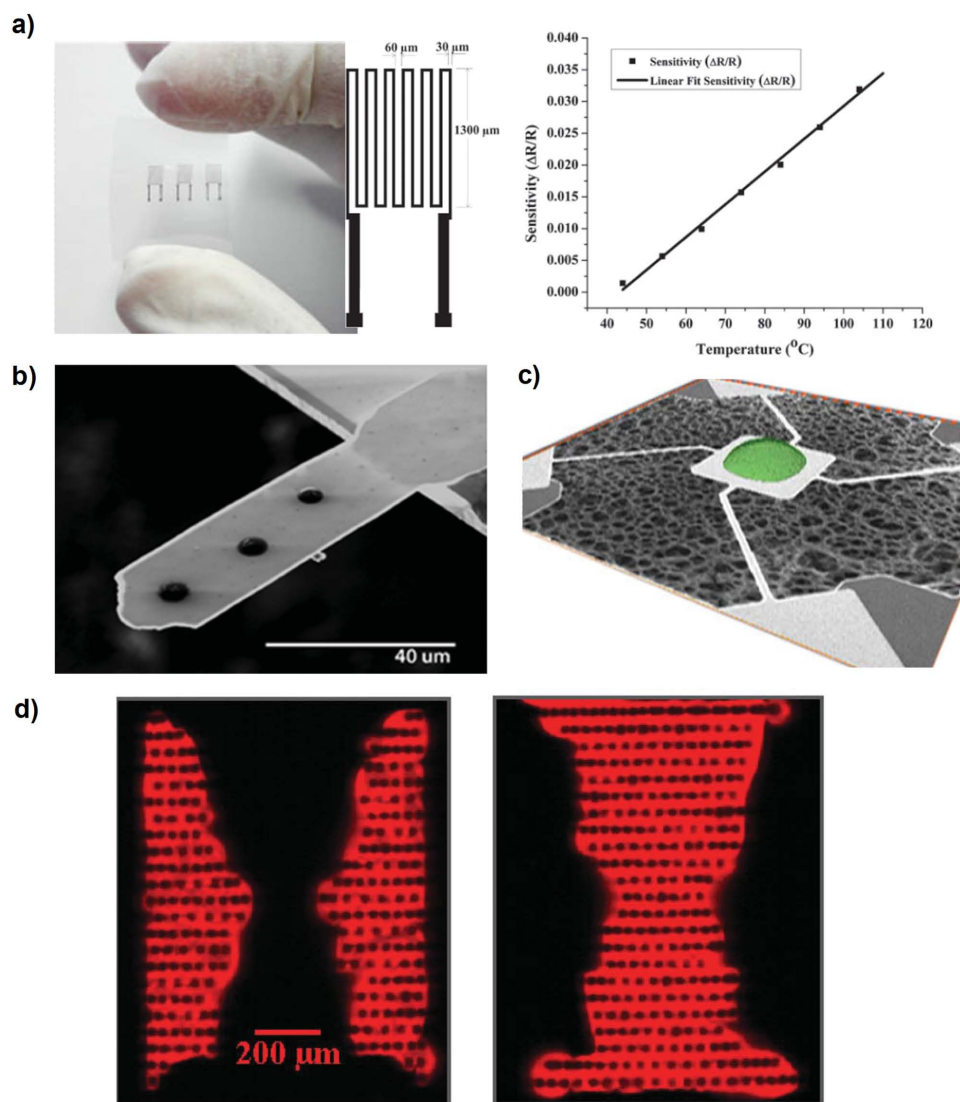


Figure 12. Fabrication of sensors and integration of analytes using electrohydrodynamic jet printing. a) Image of a flexible temperature sensor formed by electrohydrodynamic jet printing of Ag nanoparticle inks. A picture and the layout of the sensor are shown on the left. The temperature is detected by the change in the resistivity of the printed electrodes. The resistivity changes linearly with temperature (on the right). Reproduced with permission.^[110] Copyright 2014, The Japan Society of Applied Physics. b) Controlled deposition of polymers onto microcantilever gravimetric sensors for detection of multiple materials. Shown is an optical microscope image of three droplets of polyethylene printed from the melt. Reproduced with permission.^[193] Copyright 2011, IEEE. c) Analysis of the mechanical properties of hydrogel microstructures using microelectromechanical systems (MEMS) resonant sensors. The hydrogel microstructures were deposited on the sensor by electrohydrodynamic jet printing. Shown is the volume reconstruction of the hydrogel on the sensor. Reproduced with permission.^[194] Copyright 2013, Springer. d) Sensitive detection of biomolecules printed on a silicon photonic crystal using a resonance coupling laser scanning platform. Fluorescence images of the same region with two different resonance angles. The face and vase parts were printed with an oligonucleotide and a protein, respectively. The difference in the density of adsorbed molecules leads to different resonance angles. Reproduced with permission.^[195] Copyright 2013, The Royal Society of Chemistry.

interest for e-jet printing is in the fabrication of radio-frequency identification systems.^[196]

6.3. Biotechnology

Related to examples described above, e-jet printing has been explored in biotechnology, where high-resolution patterning of biomolecules and other soft materials is often needed. Due to the sensitive nature of such materials, single-step direct additive printing approaches are advantageous over conventional

lithographic methods, particularly in the case of arrays of multiple species on a single substrate.^[198,199] Several publications demonstrate the use of e-jet printing in the fabrication of DNA and protein microarrays. A second area of interest within the field of biotechnology is in controlling cell-substrate interactions for tissue engineering, drug assays, and basic studies of cell behavior. Here, patterning of materials that serve as attachment sites or as environments to support cell growth is often a goal. The possibility of patterning such materials at the nanoscale with control over their geometry and sizes in three dimensions may be a critical enabler for future applications.

6.3.1. Arrays of DNA Oligonucleotides and Proteins

Methods that allow the patterning of DNA with high spatial resolution have applications that range from genomics to nanoelectronics. Central to this interest is highly sequence specific Watson–Crick base pairing between single-stranded DNA molecules. The most established use of such base pairing in this context is in DNA microarrays,^[200] which consist of patterned spots of oligonucleotides each with a unique sequence that serves as a probe site that can recognize an analyte with a complementary sequence. This analyte could include a fluorescent molecule or a nanoparticle as a signal of the recognition event. Reducing the dimensions of each spot in such an array increases the number of recognition sites per area. Another motivation for patterning DNA oligonucleotides is in the use of self-assembled DNA nanostructures as templates for the assembly of other nanomaterials.^[201] The need for patterning multiple sequences of oligonucleotides with minimal amounts of contamination and high spatial resolution makes e-jet printing an attractive option for these purposes. Rogers and co-workers^[33] showed that DNA can be e-jet printed into different geometries with minimum feature sizes that approach ≈ 100 nm. Besides single-stranded oligonucleotides, the authors demonstrated printing of double-stranded DNA without any denaturation effects. Aptamer-based biosensing and programmed material assembly were two key capabilities enabled by e-jet printing of oligonucleotides. Results related to the latter capability appear in **Figure 13a** where the location of gold nanoparticles can be controlled through the use of particles functionalized with oligonucleotides having sequences that are complementary to the printed oligonucleotides.

Protein microarrays serve as platforms for studies of the interactions and functionalities of proteins. The complex structure of proteins and their high sensitivity to parameters such as temperature and pH create additional challenges in the formation of protein microarrays in comparison to their DNA counterparts. This same complexity, however, along with the critical roles of proteins in nearly all cellular

processes motivate the development of platforms where the sizes and geometries of printed patterns of proteins can be precisely controlled. Poellmann et al.^[202] showed that e-jet printing can be used to pattern fibronectin, an extracellular matrix protein, at a micrometer length scale on polyacrylamide substrates. An important aspect of this study was the use of soft substrates with controllable mechanical properties. Because the elasticity of the substrate plays a critical role in the interaction between the cell, the ability to pattern on such substrates represents an important capability. In another study by Shigeta et al.,^[197] patterned arrays of diverse classes of proteins such as streptavidin, IgG, fibrinogen, and γ -globulin were prepared via e-jet printing. The use of automated multinozzle print heads enabled the placement of these proteins into complex geometries on single substrates, as shown in **Figure 13b**. The experiments further revealed that the e-jet printing process does not cause any degradation of the proteins. These processes can also be performed on structured surfaces such as plasmonic^[197] and photonic^[195] crystals, thereby expanding the options in analysis of protein arrays. Similar approaches can also deliver drug molecules to specific wells for microfluidic drug-delivery systems.^[203]

6.3.2. Directing Cell–Substrate Interactions

The natural environment of a cell is complex, with topographical, chemical, and mechanical variations at length scales that range from micrometers to nanometers. Artificial substrates that can mimic certain features of natural systems are of interest for the study of cell–substrate interactions and for applications in biomedical devices and scaffolds. E-jet printing provides relevant capabilities in these contexts. In one study, Wagoner-Johnson and co-workers^[204] developed a fabrication method to pattern multiple hydrogels.^[205] As shown in **Figure 14a,b**, the process starts with e-jet printing of polyacrylamide hydrogel precursors which include monomers and crosslinkers. Following the polymerization of the printed hydrogel by exposure to UV light, a second prepolymer solution was backfilled on the patterned substrate. The hydrogel

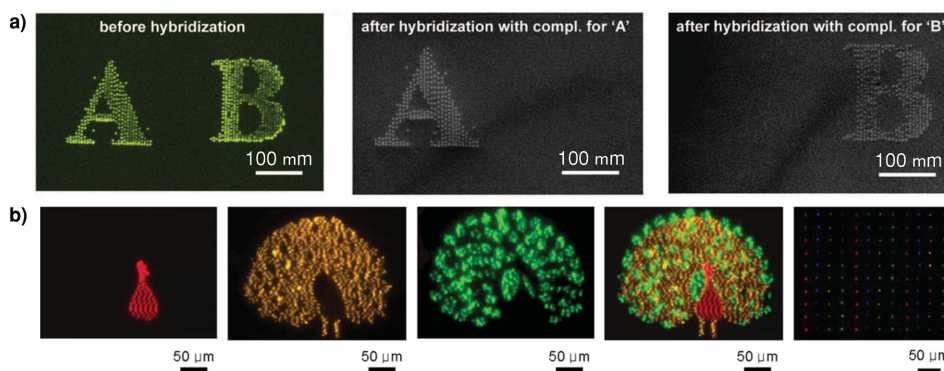


Figure 13. DNA and protein arrays. a) Printing multiple sequences of single stranded DNA molecules. Shown in the left is a fluorescence micrograph of printed letters A and B using two different sequences of single-stranded oligonucleotides. Both oligonucleotides bear the same fluorophore at the end of the strands. Selective hybridization of Au nanoparticles coated with complementary sequences leads to the SEM images (middle and right). Reproduced with permission.^[33] Copyright 2008, American Chemical Society. b) Fluorescence microscope images of a printed pattern of a peacock consisting of three different fluorescently labeled proteins. The first three fluorescence images show the parts of the pattern using channels specific to the individual fluorophores. The fourth image is generated by merging the individual images. The last fluorescence image is taken from a dot array of four different proteins. Reproduced with permission.^[197] Copyright 2012, American Chemical Society.

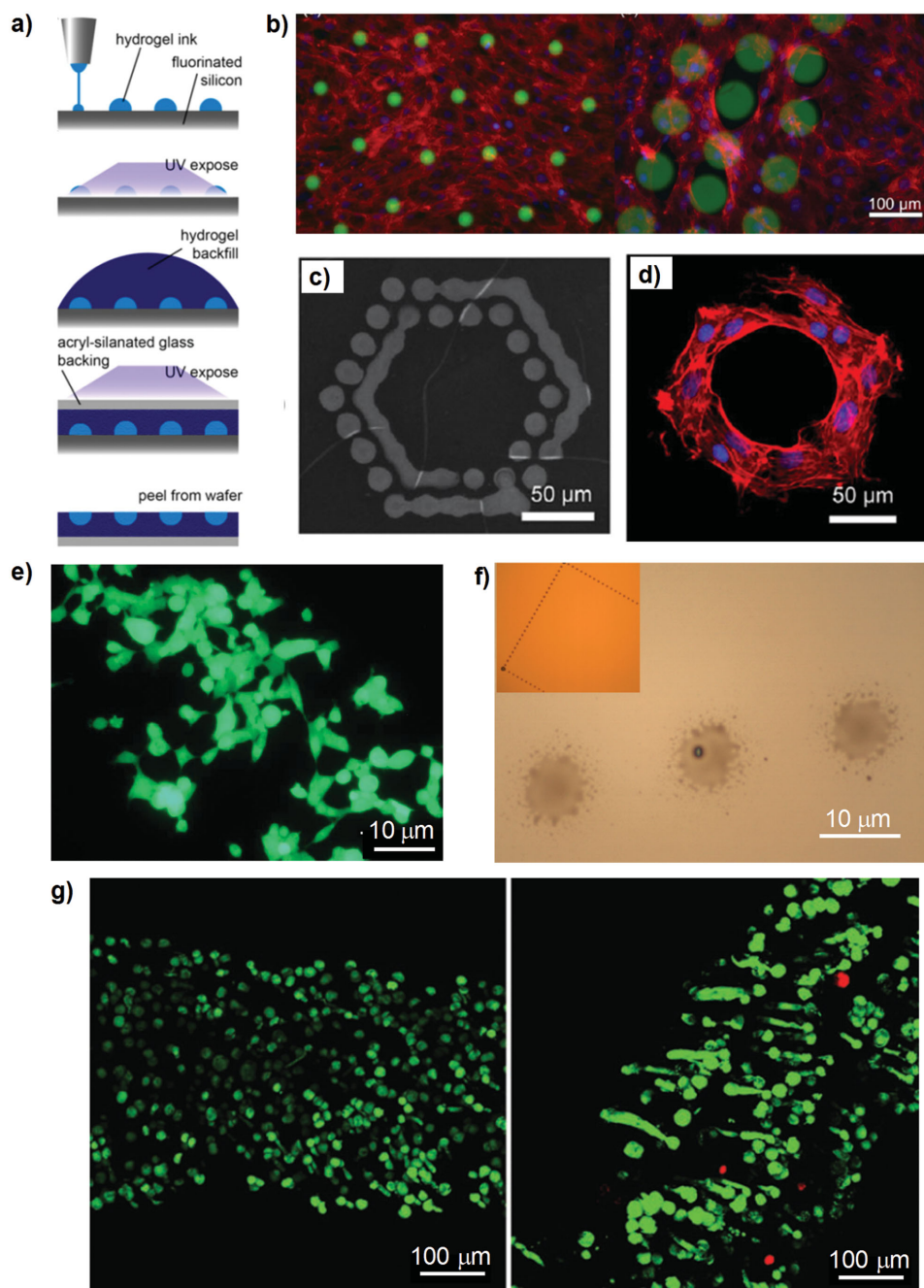


Figure 14. Controlling the spatial position of cells by electrohydrodynamic jet printing. a,b) Hydrogel patterning by printing to prepare substrates for cell culture. a) Schematic illustration of the process to define patterns of a hydrogel in a background of another hydrogel. An ink containing hydrogel prepolymers is printed on a functionalized silicon substrate and polymerized by UV light. The spaces between the printed hydrogels are backfilled with a second hydrogel material. The hydrogel is peeled from the silicon substrate and transferred to a glass substrate bringing the film upside down. b) The adhesion of cells proliferated over the fabricated hydrogel arrays described in (a). Shown is the cell behavior on small (24 μm , left) and large (70 μm , right) hydrogel spots. Reproduced with permission.^[204] Copyright 2014, IOP Publishing. c,d) Patterning proteins on hydrogel substrates to control cell adhesion. c) Immunofluorescently labeled fibronectin protein patterns printed by electrohydrodynamic jet printing. d) Fluorescence images of MC3T3-E1 cells stained with rhodaminephalloidin (red) and DAPI (blue) on the fibronectin patterns. Reproduced with permission.^[206] Copyright 2013, Springer. e) Aerodynamic assisted electro-spraying of cells. Shown is a fluorescence microscope image of the jetted HEK 293T cells. Reproduced with permission.^[208] Copyright 2008, IOP Publishing. f) Printing bacterial cells with electrohydrodynamically induced flows. An optical microscope image of the printed spots using a bacterial suspension. The inset shows the low magnification image of the patterns. Reproduced with permission.^[209] Copyright 2010, American Chemical Society. g) An electrohydrodynamic process to print suspensions containing 3T3 mouse fibroblast cells. Fluorescence microscopy images of the printed cells after 1 day (left) and 7 days (right) of culture. The green and red colors show live and dead cells, respectively. Reproduced with permission.^[210] Copyright 2014, Mary Ann Liebert, Inc.

film was placed upside down following a second photoinduced cross-linking exposure through a glass slide. This method allowed the fabrication of micrometer-sized patterns of hydrogels that consist of two different materials. The use of such a platform is demonstrated in Figure 14b, where MC3T3-E1 pre-osteoblast cells are cultured on the patterned hydrogels. The proliferation behavior of the cells depended strongly on the dimensions and geometries of the patterns. In a related report from Poellmann and Wagoner-Johnson,^[206] polyacrylamide hydrogels were functionalized with *N*-hydroxysuccinimide to provide covalent attachment of printed proteins as sites for adhesion and spreading of the cells (Figure 14c,d). An alternative approach^[207] used printed, microsized fibers of a biocompatible polymer, polycaprolactone, to study attachment and migration of fibroblast cells. The cells showed cycles of attachment and detachment to the microfibers, as revealed by time-lapse microscopy.

The direct printing of live cells represents an interesting research direction that may be enabling for a range of uses in biotechnology. Initial efforts in this direction indicate promise for e-jet printing techniques. Early work from Jayasinghe and co-workers^[211,212] demonstrated that living cells can survive the high electric fields and pressure effects associated with the jetting process. The printed cells survived without any damage and showed normal rate of cell division. The results were similar for different cell lines such as human peripheral blood monocytes, mouse CAD cells, and undifferentiated neuronal cells. The diameters of the deposited spots ranged from 200 μm to 1000 μm and contained different numbers of cells. This approach could be combined with an aerodynamic assisted jetting process to generate stable cone-jets for additional levels of control as shown in Figure 14e.^[208] In another study, Kim et al.^[209] printed bacterial cells on a bare silicon wafer with a resolution of $\approx 10 \mu\text{m}$. As shown in Figure 14f, individual *Staphylococcus epidermidis* cells appear as dark spots in optical microscopy. The residue of other components of the ink, following evaporation of the solvent, remains and surrounds the cells. This approach allows printing of cells with single-cell resolution, though some spots may have more than one cell or even no cells. In another study, Gasperini et al.^[210] printed a mixture of cells and alignate and investigated the viability of the cells via confocal microscopy, as shown in Figure 14g. The alignate cross-links on the substrate and therefore facilitates attachment of cells.

Tissue engineering represents an expanding area of development for the treatment of many types of patients. Typically, scaffolds are designed to support growth of cells,

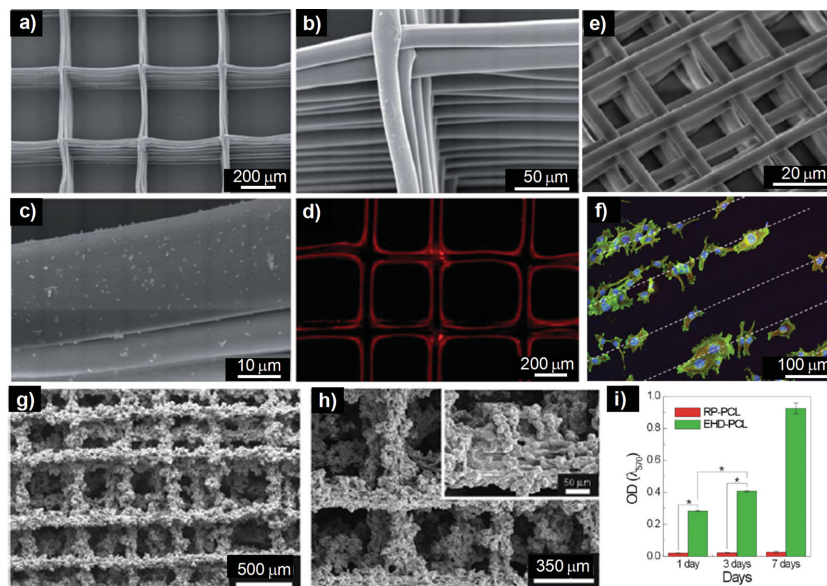


Figure 15. Fabrication of 3D scaffolds by electrohydrodynamic jet printing. a–d) 3D polycaprolactone (PCL) scaffolds for enhanced cartilage regeneration. a,b) SEM images of printed PCL scaffolds. c) SEM image of the morphology of the fibers after coating with polydopamine for the functionalization of the scaffolds. d) Collagen is grafted to increase the bioactivity of the scaffold. The presence of collagen is validated by the red color observed in fluorescence microscopy. Reproduced with permission.^[214] Copyright 2013, The Royal Society of Chemistry. e) High resolution 3D scaffold fabrication by electrohydrodynamic jet printing at elevated temperatures from melted PCL. Reproduced with permission.^[215] Copyright 2014, Elsevier. f) Patterns of nanometer hydroxyapatite by an electrohydrodynamic atomization process to guide the cell adhesion on substrates. Shown is a fluorescence microscope image of osteoblast cells on the patterns of hydroxyapatite. Reproduced with permission.^[219] Copyright 2011, Elsevier. g–i) Fabrication of porous PCL scaffolds for bone tissue regeneration using a grounded bath solution. g,h) SEM images of the highly porous printed scaffold structures. i) Cell viability is much higher in the case of printed scaffold (EHD-PCL, green) in comparison to the control scaffold (rapid prototyped PCL, RP-PCL, red). Reproduced with permission.^[220] Copyright 2011, American Chemical Society.

tissues and organs. These structures must, of course, be biocompatible but they must also offer proper mechanical properties and 3D architectures suitable for the penetration and proliferation of cells.^[213] **Figure 15** presents several examples of the use of e-jet printing to fabricate such scaffolds. Wang and co-workers^[214] fabricated 3D structures from polycaprolactone for enhanced cartilage regeneration. Here, polymer is printed from a single fiber that emerges from the nozzle, where it deposits on the substrate with controlled alignment. Sequential printing of 20 layers of fibers having diameters of 20 μm yielded the 3D scaffold structure shown in Figure 15a,b. Further functionalization of the fibers with polydopamine and collagen (Figure 15c,d) increases the attachment, spreading and viability of the cells by increasing the hydrophilicity of the polycaprolactone. In a recent study by Dong and co-workers,^[215] e-jet printing was used in combination with an extrusion deposition technique to prepare scaffolds that have features ranging between the millimeter and micrometer length scales. Thick filaments formed by extrusion provided mechanical support to thin filaments created using an e-jet printer with a heated nozzle. Figure 15e presents high resolution patterns of polycaprolactone printed from the melt using e-jet printing. The widths of the filaments were as small as 5 μm . Edirisinghe and co-workers reported

several studies^[30,216–219] on the use of e-jet printing techniques for scaffold fabrication. The authors investigated different polymers, including polycaprolactone, polyurethane, polyhedroligomeric silsesquioxane–poly(carbonate-urea) urethane, and polyhedroligomeric silsesquioxane–polycaprolactone–poly(carbonate-urea)urethane as the scaffold materials. Additional work^[218,219] also demonstrated printing of nanosized hydroxyapatite crystals, which are essential components of bone. In earlier efforts,^[218] these same authors explored the effect of printing conditions such as working distance and applied voltage on the jet formation and showed that hydroxyapatite can be printed in spraying or cone-jet modes. Line widths as small as 50 μm have been achieved using a nozzle with an inner diameter of 260 μm . Using a template assisted e-jet printing process,^[219] hydroxyapatite nanoparticles were patterned with feature sizes about 10 μm which results in guided attachment of human osteoblast cells as shown in Figure 15f. Kim and co-workers^[220] developed a modified e-jet printing process to fabricate highly porous and multilayer polycaprolactone scaffolds. In this modified setup, the solid target substrate was replaced with a bath of 5% poly(ethylene oxide) solution. The scaffolds were recovered from the solution by dissolving the PEO in water followed by a drying step. The authors found that this modification prevented crumbling of the deposited materials and allowed generation of highly porous structures in a multi-layered configuration as shown in Figure 15g–i. The viability of osteoblast-like cells was much higher on the e-jet printed scaffolds in comparison to ones fabricated by conventional rapid prototyping techniques.

6.4. Photonic and Plasmonic Devices

A promising research direction for which e-jet printing may enable new capabilities is in the fabrication of optical devices, from waveguides to light-emitting diodes (LEDs). Recent work from Alleyne and co-workers^[221] presented several such examples, including a microlens array, an optical waveguide multiplexer, and a multi-refractive index diffraction grating. The authors fabricated such devices using a UV curable ink widely used in optical systems. The ability to pattern multiple materials with high resolution is a critical advantage of e-jet printing in such applications. In another study by Cunningham and co-workers,^[222] e-jet printing was used to define channels with submicrometer heights on a photonic crystal surface, to confine the liquid volume and provide significant enhancement of the fluorescence. These channels can be easily defined due to the additive and high resolution nature of e-jet printing.

Quantum dots (QDs), which are nanoscale crystals of semiconducting materials, represent a material of interest for applications in photonics and plasmonics. The size dependent optical and electrical properties of QDs make them appealing as active or passive materials in devices. Recently, two groups independently demonstrated the power of e-jet printing techniques for high-resolution patterning of QDs. In a study by Kress et al.,^[223] nanoscale patterns of QDs were generated on flat and structured substrates using a modified e-jet

printing process^[119] based on the autofocusing of droplets, as described earlier. The authors demonstrated lines and spots with critical dimensions of 120 nm and 180 nm (Figure 16a), respectively, with this process. This resolution can be further scaled down to ≈ 30 nm spots that are sparsely located along a line using dilute inks and high stage speeds. The autofocusing effects provided a convenient way to deposit QDs with high precision on structured surfaces. For example, QDs could be printed on the apexes of gold wedges which are of interest for plasmonics. The authors also demonstrated the use of printed QDs in a plasmonic circuit by integrating gold nanostructures fabricated with lithography (Figure 16a). In other work by Kim et al.,^[224] high-resolution patterns of QDs were prepared by e-jet printing with application demonstrations in light emitting diodes (LEDs). QDs could be printed in stacked and interdigitated geometries (Figure 16b) with a resolution of a few hundred nanometers. The maximum luminance and external quantum efficiency of the LEDs were better than those of similar devices fabricated by spin-casting and/or vacuum deposition techniques. Interestingly, QDs formed highly closed packed structures in the both of the studies, probably due to inter-particle interactions in the small volumes of ink. Such work highlights the promise of high-resolution printing of QDs in an additive and material-efficient way.

Another area of interest for e-jet printing is in fabrication of metamaterials, as engineered structures with properties that are different from those seen in natural systems. The properties are determined by the unit structure whose dimensions must be controlled to match the wavelength of interest.^[226] Byun and co-workers^[225] showed that e-jet printing can be used to fabricate terahertz metamaterials with unit cell dimensions of several micrometers. The authors defined the necessary cells on a polyimide substrate using an ink based on silver nanoparticles. Encapsulation of the silver electrodes by a second polyimide layer was followed by separation of the entire layer from the silicon substrate, resulting in a free-standing, flexible terahertz metamaterial (Figure 16c,d). The fabricated metamaterial showed a resonant frequency of 0.5 THz and a refractive index of 18.4, in good agreement with simulations.

6.5. Self-assembly of Nanomaterials

The use of self-assembling materials as inks for e-jet printing may provide unique capabilities not only for engineering applications, but also for fundamental studies of self-assembly under geometric confinement. Recently, Onses et al.^[151] proposed a hybrid approach in nanofabrication that exploits high resolution e-jet printing together with self-assembly of block-copolymers (BCPs). In thin films, BCPs can form ultra-small (e.g., 5 nm) and dense (e.g., 10 nm) features. These capabilities have potential relevance to the semiconductor industry, as a means to extend the current capabilities of optical lithography systems.^[227] These materials can serve as “smart” inks that form self-assembled nanostructures within the geometries defined by e-jet printing. A unique capability of this approach for BCP thin-film studies is in the generation of multiple

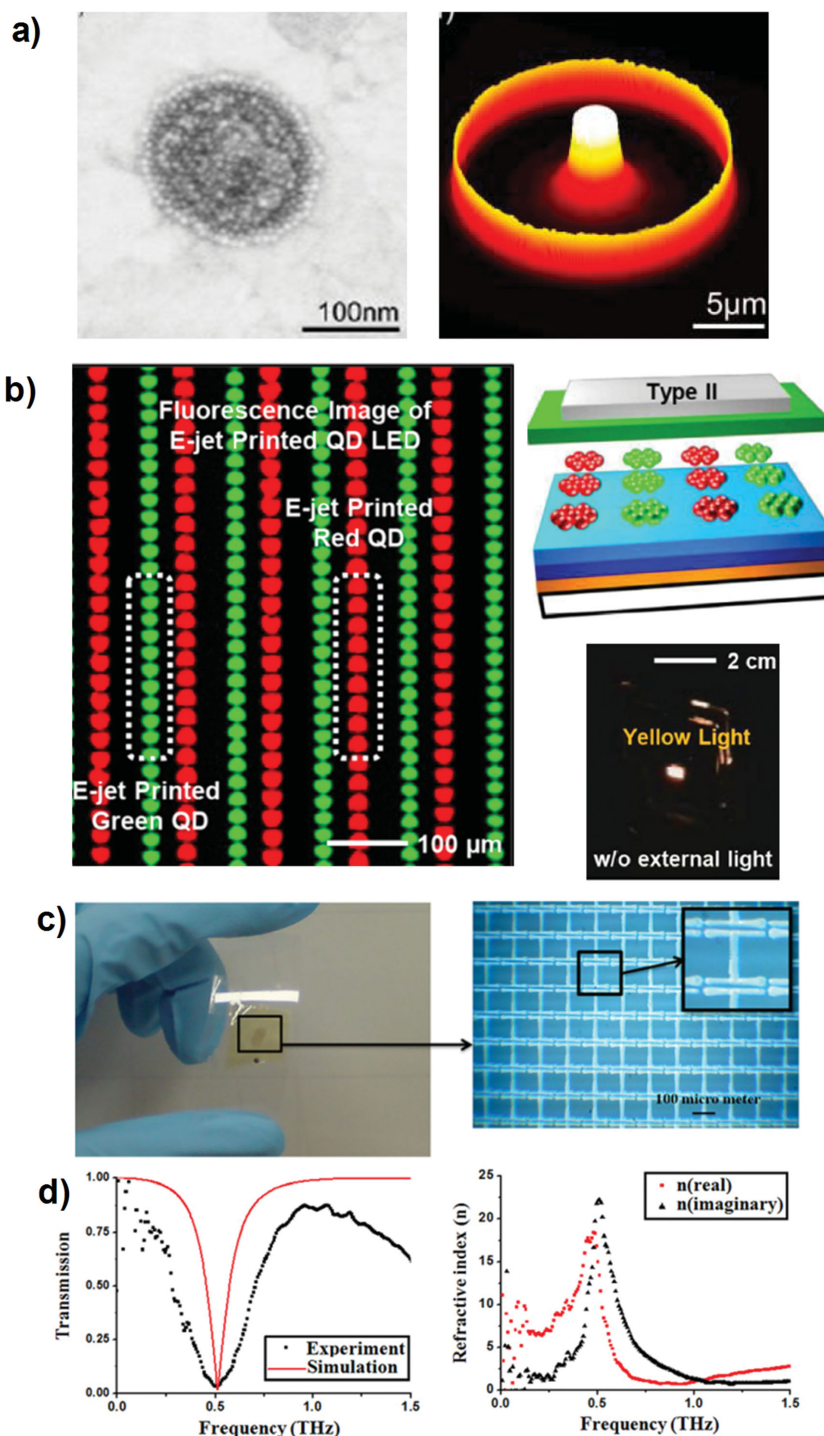


Figure 16. Optical devices by electrohydrodynamic jet printing. a) High-resolution e-jet printing of QDs on flat and structured substrates. Shown on the left is a SEM image of a printed spot of CdSe/CdS core/shell QDs. Shown on the right is the use of such printed QD arrays in a plasmonic circuit. 3D profile of scattered light in a circular gold bump fabricated by focused ion beam lithography. A printed QD spot at the center of this circle generates plasmonic waves that are then scattered in the gold structures. Reproduced with permission.^[223] Copyright 2014, American Chemical Society. b) E-jet printed QD arrays for LEDs. On the left is a fluorescence microscope image of an array of green and red QDs. Schematic illustration and photograph of the fabricated LEDs is given on the right. Reproduced with permission.^[224] Copyright 2015, American Chemical Society. c,d) Flexible terahertz metamaterials by electrohydrodynamic jet printing. c) A photograph and an optical microscope image of the fabricated metamaterial on a flexible substrate by printing Ag nanoparticles. d) Transmission and refractive index of the terahertz metamaterials. Reproduced with permission.^[225] Copyright 2013, American Institute of Physics Publishing.

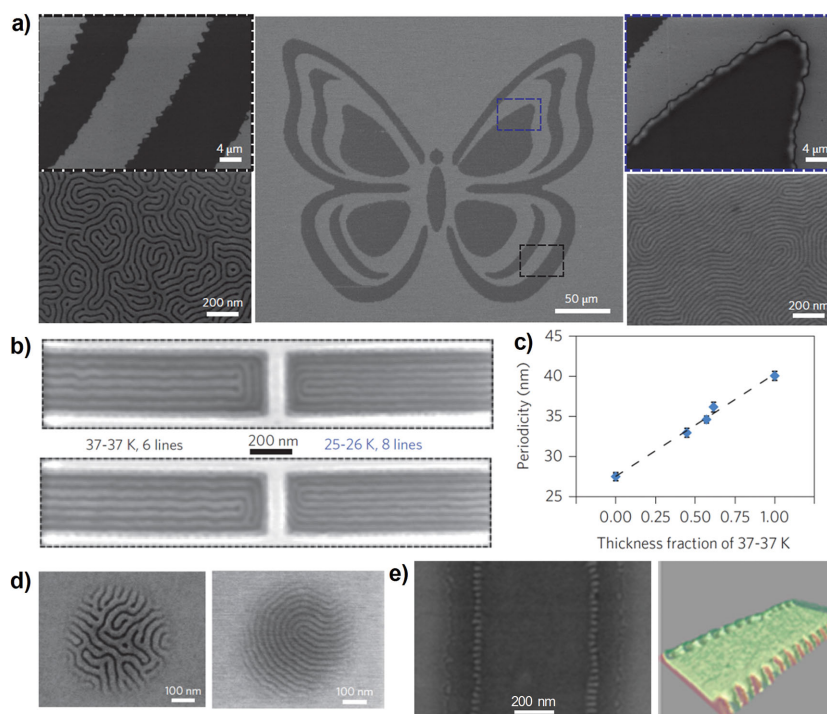


Figure 17. Printed block-copolymer (BCP) films. a) SEM images of a butterfly pattern printed with poly(styrene-*block*-methyl methacrylate) (PS-*b*-PMMA) films with two different molecular weights. The images on the left and right are magnified views of the regions printed with 37–37 kg mol⁻¹ and 25–26 kg mol⁻¹, respectively. The nanostructures form after phase-separation by thermal annealing following the printing. b) SEM image of BCP films printed onto lithographically defined trenches for directed self-assembly. The trenches were printed with 37–37 kg mol⁻¹ (left) and 25–26 kg mol⁻¹ (right) PS-*b*-PMMA. c) Continuous tuning of the periodicity of the nanoscale domains by mixing BCPs on the substrate. The plot shows the periodicity of the domains with respect to the thickness fraction of one of the components. d,e) Individual printed dots and lines for investigation of BCP self-assembly under confinement. d) SEM images of individual printed dots with different molecular weights. e) A printed line of PS-*b*-PMMA on a preferential wetting substrate. A SEM (left) and 3D simulation image of the printed BCP line. a–d, Reproduced with permission.^[151] Copyright 2013, Nature Publishing Group. e) Reproduced with permission.^[150] Copyright 2014, American Chemical Society.

nanostuctures with independently defined size, periodicity, and morphology over a single substrate. An example is presented in **Figure 17a**, where a complex image was printed using BCP inks. Here continuous BCP films can be patterned by printing lines or dots in a raster-scanning mode to define complex images. Phase separation of the BCP induced by thermal annealing leads to self-assembled nanostructures within the printed geometries. The use of inks that consist of BCPs with different molecular weights allows precise control of the size and periodicity of the self-assembled nanostructures. This approach can be integrated with common techniques for the directed self-assembly of BCPs to register individual domains with respect to the lithographically prepared templates, as shown in **Figure 17b**. The size and periodicity of the nanostructures can be continuously tuned by mixing multiple BCP inks that are printed on top of each other (**Figure 17c**). Finally, high-resolution printing of BCPs allows access to geometrically confined structures at length scales close to the size and periodicity of the domains formed by self-assembly (**Figure 17d,e**). Various confinement effects can be readily observed on such structures and can provide a vehicle for experimental and simulation^[150] studies of the fundamental effects of geometric confinement on BCP self-assembly.

Integration of another type of molecular assembly process with e-jet printing can be used to define chemical patterns on a substrate with high spatial resolution and uniformity. Polymer

brushes are macromolecules that are end grafted to a surface. E-jet printing of such end-functional polymers^[150] provides a way to control the chemical functionality of surfaces. A unique advantage of polymer brushes in this context is that the thickness of the brushes is determined by the molecular weight of the polymer. Therefore, patterns of polymer brushes can be prepared with extreme uniformity in thickness, regardless of any nonuniformities in the printing step. The dimensions and geometries of polymer brushes can be defined in the plane by printing, with a resolution that extends below 100 nm. These approaches may be useful in patterning wetting layers^[228] and functional polymers^[229,230] for different applications.

An additional research direction within this theme is in the control of particle assembly within printed patterns. This type of process can be driven by capillary forces that act on the particles during the evaporation of the printed droplets, as spontaneous organization of the materials defined solely by the printing. An early example of this approach was presented by Korkut et al.^[231] using polystyrene microspheres with an average diameter of 5.7 μm. The particles were printed from solutions that contain high-molecular-weight poly(ethylene oxide), ethanol, and water using nozzles with inner diameters as small as 340 μm. The particles self-assemble into arrays of clusters within the printed features, as shown in **Figure 18a**, as a result of capillary interactions between the particles and substrate during evaporation of the

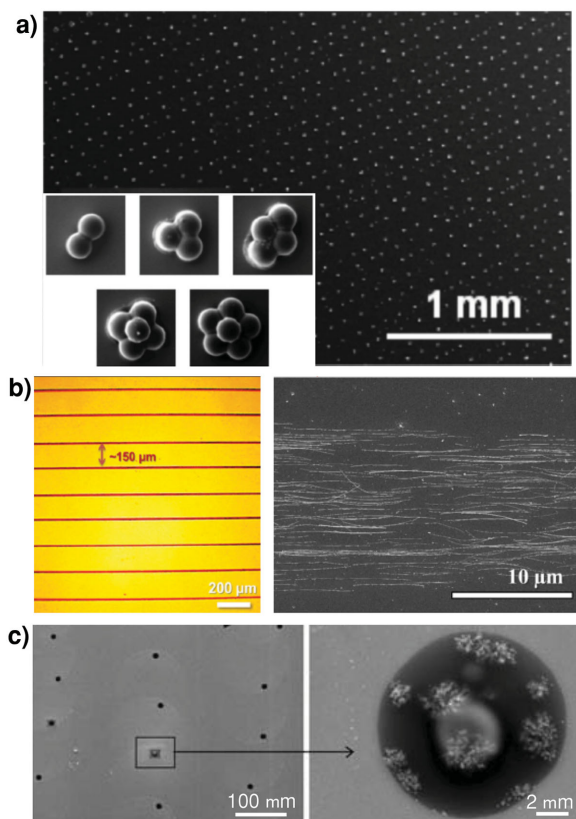


Figure 18. Assembly of particles by electrohydrodynamic jet printing. a) SEM images of linear arrays of microspheres self-assembled within the printed features. The inset shows the details of the clusters that can be achieved with the approach. The assembly is driven by capillary forces during the evaporation of the liquid in the ink. Reproduced with permission.^[231] Copyright 2008, American Chemical Society. b) Aligned Ag nanowires: an optical microscope (left) and SEM image (right) of the linear arrays of Ag nanowires. Reproduced with permission.^[232] c) Clusters of Au nanoparticles: SEM images of an array of printed dots (left) and a magnified view of the individual dots. Reproduced with permission.^[233] Copyright 2010, Springer.

liquid. These clusters included different numbers of particles with some level of deformation to fill the interstitial voids. Recently, Byun and co-workers^[232] demonstrated that silver nanowires can be aligned within the printed lines in an orientation that is parallel to the long axis of the lines. Silver nanowires with average diameters of 40 nm and lengths of

20 μm suspended in a water/ethanol solution that contains high-molecular-weight poly(ethylene oxide) served as the ink. The incorporation of poly(ethylene oxide) increased the viscosity and reduced the surface tension of the ink and aided jet formation. The concentration of silver nanowires and the flow rate were critical parameters for the width and uniformity of the e-jet printed lines. Silver nanowires aligned within the printed lines as a result of the flow and electrical field as shown in Figure 18b. Stark and Wang^[145,233] explored e-jet printing of spherical gold nanoparticles with diameters of 10 nm and found that particles form clusters within the printed spots as shown in Figure 18c. These clusters likely form due to capillary interactions between the particles during the evaporation of water. Such colloidal assemblies can be useful in photonic crystals with multiple wavelength bands as recently demonstrated with ink-jet printing.^[234]

6.6. Charge Printing

E-jet printing can be used to pattern charges on surfaces, as a complementary capability to all of the previously mentioned studies, each of which involves formation of solid material structures. Park et al.^[235] showed that negative and/or positive charges can be printed using a wide variety of ink compositions and that these charges can be retained for several days in low-humidity environments (**Figure 19**). Positive and negative charges could be printed by applying a positive and negative voltage at the nozzle with respect to a grounded substrate, respectively. Charges could be printed with a range of different inks that contain polymers, metallic nanoparticles and oligonucleotides. The authors demonstrated the use of such charges to tune the properties of silicon nanomembrane transistors, as shown in Figure 19b, where the printed charges resulted in a change of the threshold voltages through electrostatic doping effects (Figure 19c). Additional possibilities include the use of the printed charge to guide the deposition of charged particles or other material building blocks.

6.7. 3D Printing

The use of additive manufacturing processes to fabricate 3D objects represents a valuable means for the rapid prototyping

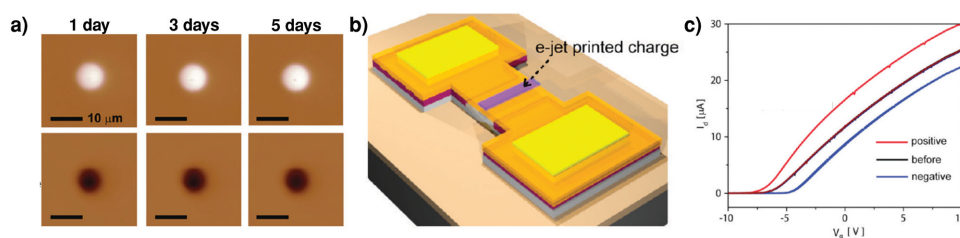


Figure 19. High-resolution charge printing. a) Printed dots of positive (top row) and negative (bottom) charges. Shown is a Kelvin force microscopy image of the charges. Each column corresponds to a different time between the printing and measurement of the charge. The patterns were printed using aqueous NaCl solution and the substrates were stored in a low humidity environment. b, c) Fabrication of devices using the charge printing. b) Schematic illustration of charge printing on the center of a transistor channel for electrostatic doping. c) Drain current (I_d) as a function of gate voltage (V_g). The threshold voltage shifts with the amount of printed charge. Reproduced with permission.^[235] Copyright 2010, American Chemical Society.

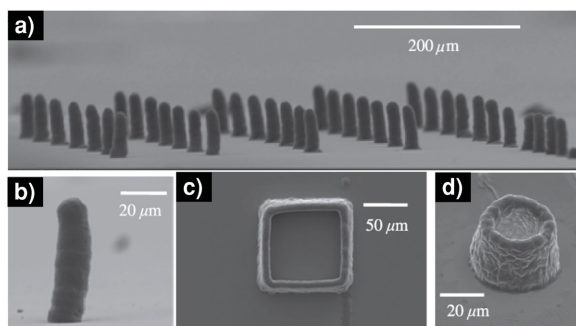


Figure 20. Electrohydrodynamic 3D printing using a phase change material (wax) as the ink. The printing system was modified with a heater to melt the wax. SEM images of various 3D structures with sub 10 μm resolution: a,b) a pillar array and a magnified view of an individual pillar with an aspect ratio ≈8, c,d) tubular structures with thin walls. Reproduced with permission.^[238] Copyright 2014, Elsevier.

and production of specialized or customized objects for industrial and household applications. Currently employed techniques such as stereolithography have resolutions on the order of 50 micrometers. Extrusion-based, direct-write 3D printing approaches developed by Lewis and co-workers can extend this resolution below 10 micrometers.^[236,237] E-jet printing has the potential to improve this resolution, but most printed structures in the literature have low aspect ratios, with limited three dimensionality. Recent work by Dong and co-workers^[238,239] showed that 3D objects can be fabricated by e-jet printing with critical dimensions smaller than 10 μm and aspect ratios as large as ≈8, as shown in **Figure 20**. An appealing aspect of this work is that the authors used wax, a material that is already used in conventional additive manufacturing systems. This material rapidly solidified following e-jet printing from a nozzle that was heated to 110 °C. Further extension of this resolution down to the nanometer length scale may provide a unique opportunity to fabricate surfaces with an extreme level of control over the structure and composition, and may be enabling in preparation of, for example, scaffolds that perfectly mimic natural systems.

7. Concluding Remarks

High-resolution, additive patterning of materials through electrohydrodynamically induced flows is an emerging capability that presents opportunities for further research with strong potential of applications in various fields. Printed electronics remain one of the most obvious areas of application, particularly for areas such as thin-film transistors,^[240] where access to length scales that cannot be directly achieved with conventional inkjet printer systems is important. For this and other areas, the continued development of functional inks that can be readily printed under electrohydrodynamic effects and which can provide patterns with a sufficient level of conductivity is critical for the advancement of the field. A range of materials such as carbon nanotubes,^[241,242] graphene,^[243] particle-free silver,^[244] and liquid metals^[245] appears promising. Expansion of these materials and substrates may lead to unusual devices such as those made of

paper^[246] and organics.^[247] Biotechnology represents another area where e-jet printing has strong potential. Additive patterning of biomaterials with high resolution in three dimensions may enable controlled cellular environments that are central to tissue engineering^[248] and biology.^[249–251] Direct and high-resolution printing of individual cells and components of an extracellular matrix may play a key role in further developments in this area.^[252] A relatively unexplored but growing area of opportunity is in the fabrication of photonic and plasmonic devices, where patterning of nano-materials at high resolution is important. The integration of e-jet printing with other approaches such as conventional lithography, inkjet printing, and self-assembling materials to develop hybrid approaches may bring unique capabilities that are not present in the individual techniques. Standardized printing systems, including control algorithms, will accelerate the development of these applications and proliferation of the technology to the broader research community.

All such applications of e-jet printing demand a detailed understanding of the underlying aspects of the process, including ink formulation, jet formation, and droplet-substrate interactions. Systematic studies that establish relationships between the fabricated patterns, the properties of ink and substrate, and the printing conditions will be highly valuable in this context. When combined with modeling approaches, such work will improve an understanding of the physical processes, including additional effects that may play prominent roles in nozzles with extreme nanoscale dimensions, and guide the development of advanced capabilities, including continued improvements in resolution, potentially well into the sub-100 nm regime, and high-density nozzle arrays for high-throughput printing.

Acknowledgements

MSO acknowledges support from Erciyes University Scientific Research Fund (FBG-2014–5376).

- [1] Y. N. Xia, J. A. Rogers, K. E. Paul, G. Whitesides, *Chem. Rev.* **1999**, *99*, 1823.
- [2] International Technology Roadmap for Semiconductors. <http://www.itrs.net/> (accessed: January, 2015).
- [3] Y. H. Wang, C. A. Mirkin, S. J. Park, *ACS Nano* **2009**, *3*, 1049.
- [4] K. J. Baeg, M. Caironi, Y. Y. Noh, *Adv. Mater.* **2013**, *25*, 4210.
- [5] D. S. Engstrom, B. Porter, M. Pacios, H. Bhaskaran, *J. Mater. Res.* **2014**, *29*, 1792.
- [6] C. Ru, J. Luo, S. R. Xie, Y. Sun, *J. Micromech. Microeng.* **2014**, *24*, 053001.
- [7] M. Singh, H. M. Haverinen, P. Dhagat, G. E. Jabbour, *Adv. Mater.* **2010**, *22*, 673.
- [8] J. R. Castrejon-Pita, W. R. S. Baxter, J. Morgan, S. Temple, G. D. Martin, I. M. Hutchings, *Atomization Spray* **2013**, *23*, 541.
- [9] E. Tekin, P. J. Smith, U. S. Schubert, *Soft Matter* **2008**, *4*, 703.
- [10] M. X. Kuang, J. X. Wang, B. Bao, F. Y. Li, L. B. Wang, L. Jiang, Y. L. Song, *Adv. Opt. Mater.* **2014**, *2*, 34.

- [11] L. B. Wang, J. X. Wang, Y. Huang, M. J. Liu, M. X. Kuang, Y. F. Li, L. Jiang, Y. L. Song, *J. Mater. Chem.* **2012**, *22*, 21405.
- [12] M. X. Kuang, L. B. Wang, Y. L. Song, *Adv. Mater.* **2014**, *26*, 6950.
- [13] N. Zhao, M. Chiesa, H. Sirringhaus, Y. N. Li, Y. L. Wu, *J. Appl. Phys.* **2007**, *101*, 064513.
- [14] M. Caironi, E. Gili, T. Sakanoue, X. Y. Cheng, H. Sirringhaus, *ACS Nano* **2010**, *4*, 1451.
- [15] H. Sirringhaus, T. Kawase, R. H. Friend, T. Shimoda, M. Inbasekaran, W. Wu, E. P. Woo, *Science* **2000**, *290*, 2123.
- [16] Y. Y. Noh, N. Zhao, M. Caironi, H. Sirringhaus, *Nat. Nanotechnol.* **2007**, *2*, 784.
- [17] J. U. Park, M. Hardy, S. J. Kang, K. Barton, K. Adair, D. K. Mukhopadhyay, C. Y. Lee, M. S. Strano, A. G. Alleyne, J. G. Georgiadis, P. M. Ferreira, J. A. Rogers, *Nat. Mater.* **2007**, *6*, 782.
- [18] O. A. Basaran, *AIChE J.* **2002**, *48*, 1842.
- [19] G. I. Taylor, *Proc. R. Soc. London A* **1964**, *280*, 383.
- [20] S. N. Jayasinghe, M. J. Edirisinghe, *Appl. Phys. Lett.* **2004**, *85*, 4243.
- [21] X. G. Zhang, O. A. Basaran, *J. Fluid Mech.* **1996**, *326*, 239.
- [22] R. T. Collins, K. Sambath, M. T. Harris, O. A. Basaran, *Proc. Natl. Acad. Sci. USA* **2013**, *110*, 4905.
- [23] V. N. Morozov, T. Y. Morozova, *Analyt. Chem.* **1999**, *71*, 3110.
- [24] O. Yogi, T. Kawakami, M. Yamauchi, J. Y. Ye, M. Ishikawa, *Anal. Chem.* **2001**, *73*, 1896.
- [25] S. N. Jayasinghe, M. J. Edirisinghe, D. Z. Wang, *Nanotechnology* **2004**, *15*, 1519.
- [26] C. H. Chen, D. A. Saville, I. A. Aksay, *Appl. Phys. Lett.* **2006**, *88*, 154104.
- [27] C. H. Chen, D. Saville, I. Aksay, *Appl. Phys. Lett.* **2006**, *89*, 124103.
- [28] D. Z. Wang, S. N. Jayasinghe, M. J. Edirisinghe, *J. Nanoparticle Res.* **2005**, *7*, 301.
- [29] H. Kawamoto, S. Umezumi, R. Koizumi, *J. Imaging Sci. Technol.* **2005**, *49*, 19.
- [30] A. Gupta, A. M. Seifalian, Z. Ahmad, M. J. Edirisinghe, M. C. Winslet, *J. Bioact. Compat. Pol.* **2007**, *22*, 265.
- [31] D. Y. Lee, Y. S. Shin, S. E. Park, T. U. Yu, J. Hwang, *Appl. Phys. Lett.* **2007**, *90*, 081905.
- [32] M. D. Paine, M. S. Alexander, K. L. Smith, M. Wang, J. P. W. Stark, *J. Aerosol. Sci.* **2007**, *38*, 315.
- [33] J. U. Park, J. H. Lee, U. Paik, Y. Lu, J. A. Rogers, *Nano Lett.* **2008**, *8*, 4210.
- [34] S. An, M. W. Lee, N. Y. Kim, C. Lee, S. S. Al-Deyab, S. C. James, S. S. Yoon, *Appl. Phys. Lett.* **2014**, *105*, 214102.
- [35] R. T. Collins, M. T. Harris, O. A. Basaran, *J. Fluid Mech.* **2007**, *588*, 75.
- [36] D. B. Bober, C. H. Chen, *J. Fluid Mech.* **2011**, *689*, 552.
- [37] K. H. Choi, K. Ali, K. Rahman, *Chin. J. Phys.* **2014**, *52*, 799.
- [38] A. Lee, H. Jin, H. W. Dang, K. H. Choi, K. H. Ahn, *Langmuir* **2013**, *29*, 13630.
- [39] R. Juraschek, F. W. Rollgen, *Int. J. Mass Spectrometry* **1998**, *177*, 1.
- [40] I. Marginean, P. Nemes, L. Parvin, A. Vertes, *Appl. Phys. Lett.* **2006**, *89*, 064104.
- [41] I. Marginean, L. Parvin, L. Heffernan, A. Vertes, *Anal. Chem.* **2004**, *76*, 4202.
- [42] L. Parvin, M. C. Galicia, J. M. Gauntt, L. M. Carney, A. B. Nguyen, E. Park, L. Heffernan, A. Vertes, *Anal. Chem.* **2005**, *77*, 3908.
- [43] H. K. Choi, J. U. Park, O. O. Park, P. M. Ferreira, J. G. Georgiadis, J. A. Rogers, *Appl. Phys. Lett.* **2008**, *92*, 123109.
- [44] S. Mishra, K. L. Barton, A. G. Alleyne, P. M. Ferreira, J. A. Rogers, *J. Micromech. Microeng.* **2010**, *20*, 95026.
- [45] U. Stachewicz, J. F. Dijkstra, C. U. Yurteri, J. C. M. Marijnissen, *Appl. Phys. Lett.* **2007**, *91*, 254109.
- [46] J. Kim, H. Oh, S. S. Kim, *J. Aerosol. Sci.* **2008**, *39*, 819.
- [47] U. Stachewicz, C. U. Yurteri, J. C. M. Marijnissen, J. F. Dijkstra, *Appl. Phys. Lett.* **2009**, *95*, 224105.
- [48] J. Choi, Y. J. Kim, S. Lee, S. U. Son, H. Ko, V. D. Nguyen, D. Byun, *Appl. Phys. Lett.* **2008**, *93*, 193508.
- [49] L. Xu, X. Wang, T. P. Lei, D. H. Sun, L. W. Lin, *Langmuir* **2011**, *27*, 6541.
- [50] H. Kim, J. Yang, J. Chung, *Jpn. J. Appl. Phys.* **2014**, *53*, 05HC03.
- [51] K. Rahman, A. Khan, N. M. Nam, K. H. Choi, D. S. Kim, *Int. J. Precis. Eng. Man.* **2011**, *12*, 663.
- [52] S. B. Q. Tran, D. Byun, V. D. Nguyen, T. S. Kang, *Phys. Rev. E* **2009**, *80*, 026318.
- [53] H. T. Yulistira, V. D. Nguyen, P. Dutta, D. Byun, *Appl. Phys. Lett.* **2010**, *96*, 023503.
- [54] H. Kim, J. Song, J. Chung, D. Hong, *J. Appl. Phys.* **2010**, *108*, 102804.
- [55] S. Lee, J. Song, H. Kim, J. Chung, *J. Aerosol. Sci.* **2012**, *52*, 89.
- [56] N. B. Bu, Y. A. Huang, Z. P. Yin, *Adv. Mater. Res.* **2013**, *684*, 352.
- [57] B. Kim, I. Kim, S. W. Joo, G. Lim, *Appl. Phys. Lett.* **2009**, *95*, 204106.
- [58] T. Deng, K. K. Varanasi, M. Hsu, N. Bhate, C. Keimel, J. Stein, M. Blohm, *Appl. Phys. Lett.* **2009**, *94*, 133109.
- [59] H. I. Kang, D. Soltman, V. Subramanian, *Langmuir* **2010**, *26*, 11568.
- [60] J. U. Park, J. A. Rogers, in *Nanomanufacturing* (Ed: S. Chen), American Scientific Publishers, USA **2010**.
- [61] W. W. Deng, A. Gomez, *Phys. Fluids* **2010**, *22*, 051703.
- [62] W. J. Scheideler, C. H. Chen, *Appl. Phys. Lett.* **2014**, *104*, 024103.
- [63] Y. J. Kim, J. Choi, S. U. Son, S. Lee, X. H. Nguyen, V. D. Nguyen, D. Byun, H. S. Ko, *Jpn. J. Appl. Phys.* **2010**, *49*, 060217.
- [64] U. Stachewicz, J. F. Dijkstra, D. Burdinski, C. U. Yurteri, J. C. M. Marijnissen, *Langmuir* **2009**, *25*, 2540.
- [65] U. Stachewicz, J. F. Dijkstra, C. U. Yurteri, J. C. M. Marijnissen, *Microfluid. Nanofluid.* **2010**, *9*, 635.
- [66] J. L. Li, *J. Aerosol. Sci.* **2005**, *36*, 373.
- [67] S. Y. Kim, Y. Kim, J. Park, J. Hwang, *J. Micromech. Microeng.* **2010**, *20*, 055009.
- [68] K. S. Kwon, D. Y. Lee, *J. Micromech. Microeng.* **2013**, *23*, 065018.
- [69] X. H. Nguyen, S. H. Lee, H. S. Ko, *Appl. Optics* **2013**, *52*, 4494.
- [70] T. P. Forbes, F. L. Degertekin, A. G. Fedorov, *Phys. Fluids* **2011**, *23*, 012104.
- [71] C. H. Chen, in *Electrokinetics and electrohydrodynamics in microsystems* (Ed: A. Ramos), Springer, Wien/New York, **2011**, pp. 177.
- [72] R. T. Collins, J. J. Jones, M. T. Harris, O. A. Basaran, *Nat. Phys.* **2008**, *4*, 149.
- [73] F. J. Higuera, S. E. Ibanez, A. J. Hijano, I. G. Loscertales, *J. Aerosol. Sci.* **2013**, *66*, 193.
- [74] W. Wei, Z. L. Gu, S. Wang, T. Fukuda, K. Kase, J. Ju, Y. Yamagata, Y. Tajima, *Particuology* **2013**, *11*, 20.
- [75] T. I. Zohdi, *Int. J. Eng. Sci.* **2013**, *62*, 157.
- [76] A. van der Bos, M. J. van der Meulen, T. Driessen, M. van den Berg, H. Reinten, H. Wijshoff, M. Versluis, D. Lohse, *Phys. Rev. Appl.* **2014**, *1*, 014004.
- [77] K. Barton, S. Mishra, A. Alleyne, P. Ferreira, J. Rogers, *Control Eng. Pract.* **2011**, *19*, 1266.
- [78] S. Mishra, K. Barton, A. Alleyne, at the 2010 American Control Conference, Baltimore, **June 2010**, pp. 6537–6542.
- [79] W. Carter, G. C. Popell, J. Samuel, S. A. Mishra, *J. Micro Nano-Manuf.* **2014**, *2*, 021005.
- [80] E. Sutanto, A. G. Alleyne, at the IEEE American Control Conference (ACC), Portland, **June 2014**, pp. 1811–1816.
- [81] D. J. Hoelzle, K. L. Barton, at the IEEE American Control Conference (ACC), Portland, **June 2014**, pp. 1805–1810.
- [82] J. Park, B. Kim, S. Y. Kim, J. Hwang, *Appl. Phys. A: Mater. Sci. Process.* **2014**, *117*, 2225.

- [83] E. Sutanto, K. Shigeta, Y. K. Kim, P. G. Graf, D. J. Hoelzle, K. L. Barton, A. G. Alleyne, P. M. Ferreira, J. A. Rogers, *J. Micro-mech. Microeng.* **2012**, *22*, 045008.
- [84] E. Sutanto, A. G. Alleyne, K. Shigeta, J. A. Rogers, K. L. Barton, at the Proc. ASME/ISCI Int. Symp. Flexible Automation, ISFA 2012, St. Louis, **June 2012**, pp.255–261.
- [85] B. Q. T. Si, D. Byun, S. Lee, *J. Aerosol Sci.* **2007**, *38*, 924.
- [86] K. H. Choi, A. Khan, K. Rahman, Y. H. Doh, D. S. Kim, K. R. Kwan, *J. Electrostat.* **2011**, *69*, 380.
- [87] K. H. Choi, K. Rahman, A. Khan, D. S. Kim, *J. Mech. Sci. Technol.* **2011**, *25*, 3053.
- [88] Y. Pan, Y. Huang, L. Guo, Y. Ding, Z. Yin, *AIP Adv.* **2015**, *5*, 047108.
- [89] C. J. Hansen, R. Saksena, D. B. Kolesky, J. J. Vericella, S. J. Kranz, G. P. Muldowney, K. T. Christensen, J. A. Lewis, *Adv. Mater.* **2013**, *25*, 96.
- [90] J. S. Lee, S. Y. Kim, Y. J. Kim, J. Park, Y. Kim, J. Hwang, *Appl. Phys. Lett.* **2008**, *93*, 243114.
- [91] K. I. Lee, B. Lim, H. Lee, S. H. Kim, C. S. Lee, J. W. Cho, S. Chung, Y. Hong, *Proc. IEEE Micr. Elect.* **2013**, 1165.
- [92] A. Khan, K. Rahman, M. T. Hyun, D. S. Kim, K. H. Choi, *Appl. Phys. A: Mater. Sci. Process.* **2011**, *104*, 1113.
- [93] A. Khan, K. Rahman, D. S. Kim, K. H. Choi, *J. Mater. Process Tech.* **2012**, *212*, 700.
- [94] J. S. Kang, I. Park, J. H. Jung, S. S. Kim, *J. Aerosol Sci.* **2013**, *55*, 25.
- [95] S. Lee, K. An, S. Son, J. Choi, *Appl. Phys. Lett.* **2013**, *103*, 133506.
- [96] L. Tse, K. Barton, *Appl. Phys. Lett.* **2014**, *104*, 143510.
- [97] C. Wei, H. T. Qin, N. A. Ramírez-Iglesias, C. P. Chiu, Y. S. Lee, J. Y. Dong, *J. Micromech. Microeng.* **2014**, *24*, 045010.
- [98] C. Wei, H. T. Qin, C. P. Chiu, Y. S. Lee, J. Y. Dong, *J. Manuf. Syst.* **2014**, doi:10.1016/j.jmsy.2014.07.005.
- [99] S. H. Hashimdeen, M. Miodownik, M. J. Edirisinghe, *Mat. Sci. Eng., C* **2013**, *33*, 3309.
- [100] V. D. Nguyen, D. Byun, *Appl. Phys. Lett.* **2009**, *94*, 173509.
- [101] D. Byun, Y. Lee, S. B. Q. Tran, V. D. Nugyen, S. Kim, B. Park, S. Lee, N. Inamdar, H. H. Bau, *Appl. Phys. Lett.* **2008**, *92*, 093507.
- [102] K. I. Lee, B. Lim, S. W. Oh, S. H. Kim, C. S. Lee, J. W. Cho, Y. Hong, at the IEEE 27th International Conference on Micro Electro Mechanical Systems (MEMS), San Francisco, **January 2014**, pp. 963–966.
- [103] D. H. Youn, S. H. Kim, Y. S. Yang, S. C. Lim, S. J. Kim, S. H. Ahn, H. S. Sim, S. M. Ryu, D. W. Shin, J. B. Yoo, *Appl. Phys. A: Mater. Sci. Process.* **2009**, *96*, 933.
- [104] V. D. Nguyen, M. G. Schrlau, S. B. Q. Tran, H. H. Bau, H. S. Ko, D. Byun, *J. Nanosci. Nanotechnol.* **2009**, *9*, 7298.
- [105] Z. Ahmad, M. Nangrejo, M. Edirisinghe, E. Stride, P. Colombo, H. B. Zhang, *Appl. Phys. A: Mater. Sci. Process.* **2009**, *97*, 31.
- [106] Z. Ahmad, M. Nangrejo, M. Rasekh, E. Stride, M. Edirisinghe, *Int. J. Mater. Form* **2013**, *6*, 281.
- [107] K. Barton, S. Mishra, K. A. Shorter, A. G. Alleyne, P. Ferreira, J. A. Rogers, *Mechatronics* **2010**, *20*, 611.
- [108] E. Sutanto, *Vision based iterative learning control for a roll to roll micro/nano-manufacturing system*, University of Illinois at Urbana-Champaign, Urbana, Illinois, **2014**.
- [109] E. Sutanto, A. G. Alleyne, P. Amer. Contr. Conf., Washington, **June 2013**, pp. 5935–5941.
- [110] K. H. Choi, M. Zubair, H. W. Dang, *Jpn. J. Appl. Phys.* **2014**, *53*, 05HB02.
- [111] Y. J. Kim, S. Y. Kim, J. S. Lee, J. Hwang, Y. J. Kim, *J. Micromech. Microeng.* **2009**, *19*, 107001.
- [112] Y. J. Kim, S. M. Lee, S. Kim, J. Hwang, Y. J. Kim, *J. Micromech. Microeng.* **2012**, *22*, 045013.
- [113] Y. J. Kim, S. Kim, J. Hwang, Y. J. Kim, *J. Micromech. Microeng.* **2013**, *23*, 065011.
- [114] O. Y. Loh, A. M. Ho, J. E. Rim, P. Kohli, N. A. Patankar, H. D. Espinosa, *P. Natl. Acad. Sci. USA* **2008**, *105*, 16438.
- [115] Y. Lovsky, A. Lewis, C. Sukenik, E. Grushka, *Anal. Bioanal. Chem.* **2010**, *396*, 133.
- [116] K. Kaisei, N. Satoh, K. Kobayashi, K. Matsushige, H. Yamada, *Nanotechnology* **2011**, *22*, 175301.
- [117] K. Kaisei, K. Kobayashi, K. Matsushige, H. Yamada, *J. Appl. Phys.* **2012**, *111*, 074319.
- [118] S. An, C. Stambaugh, G. Kim, M. Lee, Y. Kim, K. Lee, W. Jhe, *Nanoscale* **2012**, *4*, 6493.
- [119] P. Galliker, J. Schneider, H. Eghlidi, S. Kress, V. Sandoghdar, D. Poulidakos, *Nat. Commun.* **2012**, *3*, 890.
- [120] P. Galliker, J. Schneider, D. Poulidakos, *Appl. Phys. Lett.* **2014**, *104*, 073105.
- [121] N. C. Schirmer, C. Kullmann, M. S. Schmid, B. R. Burg, T. Schwamb, D. Poulidakos, *Adv. Mater.* **2010**, *22*, 4701.
- [122] P. Ferraro, S. Coppola, S. Grilli, M. Paturzo, V. Vespini, *Nat. Nanotechnol.* **2010**, *5*, 429.
- [123] S. Grilli, S. Coppola, V. Vespini, F. Merola, A. Finizio, P. Ferraro, *P. Natl. Acad. Sci. USA* **2011**, *108*, 15106.
- [124] S. Y. Min, T. S. Kim, B. J. Kim, H. Cho, Y. Y. Noh, H. Yang, J. H. Cho, T. W. Lee, *Nat. Commun.* **2013**, *4*, 1773.
- [125] N. C. Schirmer, T. Schwamb, B. R. Burg, N. Hotz, D. Poulidakos, *Appl. Phys. Lett.* **2009**, *95*, 033111.
- [126] N. C. Schirmer, S. Strohle, M. K. Tiwari, D. Poulidakos, *Adv. Funct. Mater.* **2011**, *21*, 388.
- [127] J. A. Rogers, U. Paik, *Nat. Nanotechnol.* **2010**, *5*, 385.
- [128] O. Gennari, L. Battista, B. Silva, S. Grilli, L. Miccio, V. Vespini, S. Coppola, P. Orlando, L. Aprin, P. Slangen, P. Ferraro, *Appl. Phys. Lett.* **2015**, *106*, 054103.
- [129] V. Vespini, S. Coppola, S. Grilli, M. Paturzo, P. Ferraro, *Meas. Sci. Technol.* **2013**, *24*, 045203.
- [130] I. A. Grimaldi, S. Coppola, F. Loffredo, F. Villani, G. Nenna, C. Minarini, V. Vespini, L. Miccio, S. Grilli, P. Ferraro, *Appl. Optics* **2013**, *52*, 7699.
- [131] S. Coppola, V. Vespini, G. Nasti, O. Gennari, S. Grilli, M. Ventre, M. Iannone, P. A. Netti, P. Ferraro, *Chem. Mater.* **2014**, *26*, 3357.
- [132] M. de Angelis, P. Matteini, F. Ratto, R. Pini, S. Coppola, S. Grilli, V. Vespini, P. Ferraro, *Appl. Phys. Lett.* **2013**, *103*, 163112.
- [133] D. Li, Y. N. Xia, *Adv. Mater.* **2004**, *16*, 1151.
- [134] Y. A. Huang, X. M. Wang, Y. Q. Duan, N. B. Bu, Z. P. Yin, *Soft Matter* **2012**, *8*, 8302.
- [135] C. Song, J. A. Rogers, J. M. Kim, H. Ahn, *Macromol. Res.* **2015**, *23*, 118.
- [136] Y. A. Huang, Y. Q. Duan, Y. J. Ding, N. B. Bu, Y. Q. Pan, N. S. Lu, Z. P. Yin, *Sci. Rep.* **2014**, *4*, 5949.
- [137] Y. A. Huang, N. B. Bu, Y. Q. Duan, Y. Q. Pan, H. M. Liu, Z. P. Yin, Y. L. Xiong, *Nanoscale* **2013**, *5*, 12007.
- [138] S. K. Hwang, S. Y. Min, I. Bae, S. M. Cho, K. L. Kim, T. W. Lee, *C. Park, Small* **2014**, *10*, 1976.
- [139] Y. Lee, T. S. Kim, S. Y. Min, W. Xu, S. H. Jeong, H. K. Seo, T. W. Lee, *Adv. Mater.* **2014**, *26*, 8010.
- [140] P. R. Chiarot, P. Sullivan, R. Ben Mrad, *J. Microelectromech. S* **2011**, *20*, 1241.
- [141] A. Jaworek, A. T. Sobczyk, *J. Electrostat.* **2008**, *66*, 197.
- [142] M. N. Awais, J. D. Jo, K. H. Choi, *Appl. Phys. A: Mater. Sci. Process.* **2013**, *113*, 89.
- [143] Y. J. Kwack, W. S. Choi, *Electron. Mater. Lett.* **2012**, *8*, 341.
- [144] H. Q. Hu, S. Rangou, M. Kim, P. Gopalan, V. Filiz, A. Avgeropoulos, C. O. Osuji, *ACS Nano* **2013**, *7*, 2960.
- [145] K. Wang, J. P. W. Stark, *Anal. Chim. Acta* **2010**, *679*, 81.
- [146] H. X. Duan, C. Li, W. W. Yang, B. Lojewski, L. N. An, W. W. Deng, *J. Microelectromech. S* **2013**, *22*, 1.
- [147] E. Saleh, M. Praeger, A. S. Vaughan, W. Stewart, W. H. Loh, *J. Nanopart. Res.* **2012**, *14*, 1220.
- [148] J. S. Hong, B. S. Lee, D. Moon, J. G. Lee, I. S. Kang, *Electrophoresis* **2010**, *31*, 1357.

- [149] F. F. Wang, F. Fei, L. Q. Liu, H. B. Yu, P. Yu, Y. C. Wang, G. B. Lee, W. Jung, *Appl. Phys. Lett.* **2014**, *104*, 264103.
- [150] M. S. Onses, A. Ramirez-Hernandez, S. M. Hur, E. Sutanto, L. Williamson, A. G. Alleyne, P. F. Nealey, J. J. de Pablo, J. A. Rogers, *ACS Nano* **2014**, *8*, 6606.
- [151] M. S. Onses, C. Song, L. Williamson, E. Sutanto, P. M. Ferreira, A. G. Alleyne, P. F. Nealey, H. Ahn, J. A. Rogers, *Nat. Nanotechnol.* **2013**, *8*, 667.
- [152] J. Perelaer, P. J. Smith, D. Mager, D. Soltman, S. K. Volkman, V. Subramanian, J. G. Korvink, U. S. Schubert, *J. Mater. Chem.* **2010**, *20*, 8446.
- [153] A. Kamyshny, S. Magdassi, *Small* **2014**, *10*, 3515.
- [154] H. Klauk, *Chem. Soc. Rev.* **2010**, *39*, 2643.
- [155] T. Sekitani, T. Someya, *Jpn. J. Appl. Phys.* **2012**, *51*, 100001.
- [156] H. J. Gysling, *Curr. Opin. Colloid Interface Sci.* **2014**, *19*, 155.
- [157] H. W. Choi, T. L. Zhou, M. Singh, G. E. Jabbour, *Nanoscale* **2015**, *7*, 3338.
- [158] D. Y. Lee, J. C. Lee, Y. S. Shin, S. E. Park, T. U. Yu, Y. J. Kim, J. Hwang, N. Green, *Electrostatics 2007* **2009**, *142*, 012039.
- [159] K. Wang, M. D. Paine, J. P. W. Stark, *J. Appl. Phys.* **2009**, *106*, 024907.
- [160] K. Wang, M. D. Paine, J. P. W. Stark, *J. Mater. Sci.—Mater. Electron.* **2009**, *20*, 1154.
- [161] D. Y. Lee, D. H. Lim, Y. J. Kim, J. Hwang, *J. Imaging Sci. Technol.* **2009**, *53*, 041203.
- [162] K. Wang, J. P. W. Stark, *Appl. Phys. A: Mater. Sci. Process.* **2010**, *99*, 763.
- [163] K. Wang, M. D. Paine, J. P. W. Stark, *Optoelectron. Adv. Mater.* **2010**, *4*, 365.
- [164] X. Wang, L. Xu, G. F. Zheng, W. Cheng, D. H. Sun, *Sci. China Technol. Sc.* **2012**, *55*, 1603.
- [165] K. Wang, J. P. W. Stark, *J. Coat. Technol. Res.* **2012**, *9*, 317.
- [166] F. D. Prasetyo, H. T. Yulistira, V. D. Nguyen, D. Byun, *J. Micro-mech. Microeng.* **2013**, *23*, 095028.
- [167] K. Rahman, K. Ali, N. M. Muhammad, M. T. Hyun, K. H. Choi, *Appl. Phys. A: Mater. Sci. Process.* **2013**, *111*, 593.
- [168] S. Son, S. Lee, J. Choi, *J. Electrostat.* **2014**, *72*, 70.
- [169] T. I. Zohdi, *Comput. Mech.* **2014**, *54*, 171.
- [170] J. M. Song, at the 2014 International Conference on Electronics Packaging (ICEP), Toyama, **April 2014**, pp. 140–143.
- [171] J. Kang, Y. Jang, Y. Kim, S. H. Cho, J. Suhr, B. H. Hong, J. B. Choi, D. Byun, *Nanoscale* **2015**, *7*, 6567.
- [172] B. Seong, H. Yoo, V. D. Nguyen, Y. Jang, C. Ryu, D. Byun, *J. Micro-mech. Microeng.* **2014**, *24*, 097002.
- [173] J. Park, J. Hwang, *J. Phys. D Appl. Phys.* **2014**, *47*, 405102.
- [174] K. Rahman, A. Khan, N. M. Muhammad, J. Jo, K. H. Choi, *J. Micro-mech. Microeng.* **2012**, *22*, 065012.
- [175] D. S. Kim, K. Rahman, A. Khan, K. H. Choi, *Mater. Manuf. Process.* **2012**, *27*, 1295.
- [176] S. Jeong, S. H. Lee, Y. Jo, S. S. Lee, Y. H. Seo, B. W. Ahn, G. Kim, G. E. Jang, J. U. Park, B. H. Ryu, Y. Choi, *J. Mater. Chem. C* **2013**, *1*, 2704.
- [177] D. K. Kang, M. W. Lee, H. Y. Kim, S. C. James, S. S. Yoon, *J. Aerosol Sci.* **2011**, *42*, 621.
- [178] M. W. Lee, S. An, N. Y. Kim, J. H. Seo, J. Y. Huh, H. Y. Kim, S. S. Yoon, *Exp. Therm. Fluid Sci.* **2013**, *46*, 103.
- [179] J. K. He, F. Y. Xu, Y. Cao, Y. X. Liu, D. C. Li, Z. M. Jin, *Appl. Phys. Lett.* **2014**, *105*, 253109.
- [180] S. Lee, J. Kim, J. Choi, H. Park, J. Ha, Y. Kim, J. A. Rogers, U. Paik, *Appl. Phys. Lett.* **2012**, *100*, 102108.
- [181] S. Jeong, J. Y. Lee, S. S. Lee, Y. H. Seo, S. Y. Kim, J. U. Park, B. H. Ryu, W. Yang, J. Moon, Y. Choi, *J. Mater. Chem. C* **2013**, *1*, 4236.
- [182] Y. J. Kwack, W. S. Choi, *IEEE Electr. Device Lett.* **2013**, *34*, 78.
- [183] Y. G. Lee, W. S. Choi, *ACS Appl. Mater. Interfaces* **2014**, *6*, 11167.
- [184] T. Sekitani, Y. Noguchi, U. Zschieschang, H. Klauk, T. Someya, *Proc. Natl. Acad. Sci. USA* **2008**, *105*, 4976.
- [185] M. N. Awais, H. C. Kim, Y. H. Doh, K. H. Choi, *Thin Solid Films* **2013**, *536*, 308.
- [186] K. H. Choi, M. N. Awais, *J. Korean Phys. Soc.* **2012**, *61*, 119.
- [187] N. Duraisamy, N. M. Muhammad, H. C. Kim, J. D. Jo, K. H. Choi, *Thin Solid Films* **2012**, *520*, 5070.
- [188] S. U. Byun, H. G. Park, K. I. Lee, B. J. Lim, H. J. Lee, D. S. Seo, *Electrochem. Solid St.* **2012**, *15*, J28.
- [189] H. G. Park, S. U. Byun, H. C. Jeong, J. W. Lee, D. S. Seo, *ECS Solid State Lett.* **2013**, *2*, R52.
- [190] S. Y. Back, C. H. Song, S. Yu, H. J. Lee, B. S. Kim, N. Y. Yang, S. H. Jeong, H. Ahn, *J. Nanosci. Nanotechnol.* **2012**, *12*, 446.
- [191] H. Lee, B. Kim, C. Park, J. Y. Lee, S. Oh, N. Yang, J. Kim, S. Jeong, S. Hong, *2009 Sid International Symposium Digest of Technical Papers* **2009**, *40*, 1342.
- [192] C. H. Song, S. Y. Back, S. I. Yu, H. J. Lee, B. S. Kim, N. Y. Yang, S. H. Jeong, H. Ahn, *J. Nanosci. Nanotechnol.* **2012**, *12*, 475.
- [193] J. H. Pikul, P. Graf, S. Mishra, K. Barton, Y. K. Kim, J. A. Rogers, A. Alleyne, P. M. Ferreira, W. P. King, *IEEE Sens. J.* **2011**, *11*, 2246.
- [194] E. A. Corbin, L. J. Millet, J. H. Pikul, C. L. Johnson, J. G. Georgiadis, W. P. King, R. Bashir, *Biomed. Microdevices* **2013**, *15*, 311.
- [195] S. George, V. Chaudhery, M. Lu, M. Takagi, N. Amro, A. Pokhriyal, Y. F. Tan, P. Ferreira, B. T. Cunningham, *Lab Chip* **2013**, *13*, 4053.
- [196] S. Kim, C. Mariotti, F. Alimenti, P. Mezzanotte, A. Georgiadis, A. Collado, L. Roselli, M. M. Tentzeris, *IEEE Microw. Mag.* **2013**, *14*, 66.
- [197] K. Shigeta, Y. He, E. Sutanto, S. Kang, A. P. Le, R. G. Nuzzo, A. G. Alleyne, P. N. Ferreira, Y. Lu, J. A. Rogers, *Anal. Chem.* **2012**, *84*, 10012.
- [198] G. Arrabito, B. Pignataro, *Anal. Chem.* **2012**, *84*, 5450.
- [199] M. S. Onses, P. Pathak, C. C. Liu, F. Cerrina, P. F. Nealey, *ACS Nano* **2011**, *5*, 7899.
- [200] A. Sassolas, B. D. Leca-Bouvier, L. J. Blum, *Chem. Rev.* **2008**, *108*, 109.
- [201] A. V. Pinheiro, D. R. Han, W. M. Shih, H. Yan, *Nat. Nanotechnol.* **2011**, *6*, 763.
- [202] M. J. Poellmann, K. L. Barton, S. Mishra, A. J. W. Johnson, *Macromol. Biosci.* **2011**, *11*, 1164.
- [203] T. H. Hwang, J. B. Kim, D. S. Yang, Y. I. Park, W. Ryu, *J. Micromech. Microeng.* **2013**, *23*, 035012.
- [204] M. J. Poellmann, A. J. W. Johnson, *Biofabrication* **2014**, *6*, 035018.
- [205] K. Y. Lee, D. J. Mooney, *Chem. Rev.* **2001**, *101*, 1869.
- [206] M. J. Poellmann, A. J. W. Johnson, *Cell. Mol. Bioeng.* **2013**, *6*, 299.
- [207] M. Rasekh, Z. Ahmad, C. C. Frangos, L. Bozec, M. Edirisinghe, R. M. Day, *Acta Biomater.* **2013**, *9*, 5052.
- [208] A. Kwok, S. Arumuganathar, S. Irvine, J. R. McEwan, S. N. Jayasinghe, *Biomed. Mater.* **2008**, *3*, 025008.
- [209] K. Kim, B. U. Lee, G. B. Hwang, J. H. Lee, S. Kim, *Anal. Chem.* **2010**, *82*, 2109.
- [210] L. Gasperini, D. Maniglio, A. Motta, C. Migliaresi, *Tissue Eng. Pt. C-Meth.* **2014**, *21*, 123.
- [211] S. N. Jayasinghe, A. N. Qureshi, P. A. M. Eagles, *Small* **2006**, *2*, 216.
- [212] P. A. M. Eagles, A. N. Qureshi, S. N. Jayasinghe, *Biochem. J.* **2006**, *394*, 375.
- [213] F. J. O'Brien, *Mater. Today* **2011**, *14*, 88.
- [214] Y. L. Cai, J. L. Li, C. K. Poh, H. C. Tan, E. S. Thian, J. Y. H. Fuh, J. Sun, B. Y. Tay, W. Wang, *J. Mater. Chem. B* **2013**, *1*, 5971.
- [215] C. Wei, J. Y. Dong, *J. Manuf. Process.* **2014**, *16*, 257.
- [216] Z. Ahmad, M. Rasekh, M. Edirisinghe, *Macromol. Mater. Eng.* **2010**, *295*, 315.
- [217] M. Rasekh, Z. Ahmad, R. Day, A. Wickham, M. Edirisinghe, *Adv. Eng. Mater.* **2011**, *13*, B296.
- [218] Z. Ahmad, E. S. Thian, J. Huang, M. J. Edirisinghe, S. M. Best, S. N. Jayasinghe, W. Bonfield, R. A. Brooks, N. Rushton, *J. Mater. Sci. Mater. Med.* **2008**, *19*, 3093.

- [219] X. A. Li, J. Huang, M. Edirisinghe, W. Bonfield, *Colloid Surf. B* **2011**, *82*, 562.
- [220] S. H. Ahn, H. J. Lee, G. H. Kim, *Biomacromolecules* **2011**, *12*, 4256.
- [221] E. Sutanto, Y. Tan, M. S. Onses, B. T. Cunningham, A. G. Alleyne, *Manuf. Lett.* **2014**, *2*, 4.
- [222] Y. F. Tan, E. Sutanto, A. G. Alleyne, B. T. Cunningham, *J. Biophotonics* **2014**, *7*, 266.
- [223] S. J. P. Kress, P. Richner, S. V. Jayanti, P. Galliker, D. K. Kim, D. Poulidakos, D. J. Norris, *Nano Lett.* **2014**, *14*, 5827.
- [224] B. H. Kim, M. S. Onses, J. B. Lim, S. Nam, N. Oh, H. Kim, K. J. Yu, J. W. Lee, J. H. Kim, S. K. Kang, C. H. Lee, J. Lee, J. H. Shin, N. H. Kim, C. Leal, M. Shin, J. A. Rogers, *Nano Lett.* **2015**, *15*, 969.
- [225] H. T. Yulistira, A. P. Tenggara, V. D. Nguyen, T. T. Kim, F. D. Prasetyo, C. G. Choi, M. Choi, D. Byun, *Appl. Phys. Lett.* **2013**, *103*, 211106.
- [226] W. J. Padilla, D. N. Basov, D. R. Smith, *Mater. Today* **2006**, *9*, 28.
- [227] C. M. Bates, M. J. Maher, D. W. Janes, C. J. Ellison, C. G. Willson, *Macromolecules* **2014**, *47*, 2.
- [228] D. L. Tian, Y. L. Song, L. Jiang, *Chem. Soc. Rev.* **2013**, *42*, 5184.
- [229] Z. H. Nie, E. Kumacheva, *Nat. Mater.* **2008**, *7*, 277.
- [230] M. S. Onses, P. F. Nealey, *Small* **2013**, *9*, 4168.
- [231] S. Korkut, D. A. Saville, I. A. Aksay, *Langmuir* **2008**, *24*, 12196.
- [232] H. Lee, B. Seong, J. Kim, Y. Jang, D. Byun, *Small* **2014**, *10*, 3918.
- [233] K. Wang, J. P. W. Stark, *J. Nanopart. Res.* **2010**, *12*, 707.
- [234] L. Y. Cui, Y. F. Li, J. X. Wang, E. T. Tian, X. Y. Zhang, Y. Z. Zhang, Y. L. Song, L. Jiang, *J. Mater. Chem.* **2009**, *19*, 5499.
- [235] J. U. Park, S. Lee, S. Unarunotai, Y. G. Sun, S. Dunham, T. Song, P. M. Ferreira, A. G. Alleyne, U. Paik, J. A. Rogers, *Nano Lett.* **2010**, *10*, 584.
- [236] B. Y. Ahn, E. B. Duoss, M. J. Motala, X. Y. Guo, S. I. Park, Y. J. Xiong, J. Yoon, R. G. Nuzzo, J. A. Rogers, J. A. Lewis, *Science* **2009**, *323*, 1590.
- [237] J. N. H. Shepherd, S. T. Parker, R. F. Shepherd, M. U. Gillette, J. A. Lewis, R. G. Nuzzo, *Adv. Funct. Mater.* **2011**, *21*, 47.
- [238] Y. Han, C. Wei, J. Y. Dong, *Manuf. Lett.* **2014**, *2*, 96.
- [239] C. Wei, J. Y. Dong, *J. Manuf. Sci. E-TASME* **2014**, *136*, 061010.
- [240] R. A. Street, *Adv. Mater.* **2009**, *21*, 2007.
- [241] T. Someya, *Nat. Nanotechnol.* **2009**, *4*, 143.
- [242] M. Kanungo, H. Lu, G. G. Malliaras, G. Blanchet, *Science* **2009**, *323*, 234.
- [243] B. W. An, K. Kim, M. Kim, S. Y. Kim, S. H. Hur, J. U. Park, *Small* **2015**, *11*, 2263.
- [244] S. B. Walker, J. A. Lewis, *J. Am. Chem. Soc.* **2012**, *134*, 1419.
- [245] C. Ladd, J. H. So, J. Muth, M. D. Dickey, *Adv. Mater.* **2013**, *25*, 5081.
- [246] D. Tobjork, R. Osterbacka, *Adv. Mater.* **2011**, *23*, 1935.
- [247] T. Sekitani, T. Someya, *Adv. Mater.* **2010**, *22*, 2228.
- [248] H. Bae, H. H. Chu, F. Edalat, J. M. Cha, S. Sant, A. Kashyap, A. F. Ahari, C. H. Kwon, J. W. Nichol, S. Manoucheri, B. Zamanian, Y. D. Wang, A. Khademhosseini, *J. Tissue Eng. Regen. M.* **2014**, *8*, 1.
- [249] Y. Shao, J. Fu, *Adv. Mater.* **2014**, *26*, 1494.
- [250] S. Ankam, B. K. K. Teo, M. Kukumberg, E. K. Yim, *Organogenesis* **2013**, *9*, 128.
- [251] J. Hong, J. B. Edel, A. J. deMello, *Drug Discov. Today* **2009**, *14*, 134.
- [252] D. Poncelet, P. de Vos, N. Suter, S. N. Jayasinghe, *Adv. Healthc. Mater.* **2012**, *1*, 27.

Received: February 28, 2015
Revised: April 20, 2015
Published online: June 29, 2015